

# Elucidating Galaxy Assembly Bias in SDSS

Andrés N. SALCEDO<sup>1</sup>, Ying ZU<sup>2,3\*</sup>, Youcai ZHANG<sup>4</sup>, Huiyuan WANG<sup>5,6</sup>,  
Xiaohu YANG<sup>2,3,7</sup>, Yiheng WU<sup>4</sup>, Yipeng JING<sup>2,3,7</sup>, Houjun MO<sup>8</sup>, and David H. WEINBERG<sup>1</sup>

<sup>1</sup>*Department of Astronomy and Center for Cosmology and AstroParticle Physics,  
The Ohio State University, Columbus, OH 43210, USA;*

<sup>2</sup>*Department of Astronomy, School of Physics and Astronomy, Shanghai Jiao Tong University, Shanghai 200240, China;*

<sup>3</sup>*Shanghai Key Laboratory for Particle Physics and Cosmology, Shanghai Jiao Tong University, Shanghai 200240, China;*

<sup>4</sup>*Key Laboratory for Research in Galaxies and Cosmology, Shanghai Astronomical Observatory, Shanghai 200030, China;*

<sup>5</sup>*CAS Key Laboratory for Research in Galaxies and Cosmology, Department of Astronomy,  
University of Science and Technology of China, Hefei, Anhui 230026, China;*

<sup>6</sup>*School of Astronomy and Space Science, University of Science and Technology of China, Hefei 230026, China;*

<sup>7</sup>*Tsung-Dao Lee Institute, Shanghai Jiao Tong University, Shanghai 200240, China;*

<sup>8</sup>*Department of Astronomy, University of Massachusetts Amherst, MA 01003, USA*

Received January 11, 2022; accepted April 6, 2022

We investigate the level of galaxy assembly bias in the Sloan Digital Sky Survey (SDSS) main galaxy sample using ELUCID, a state-of-the-art constrained simulation that accurately reconstructed the initial density perturbations within the SDSS volume. On top of the ELUCID haloes, we develop an extended HOD model that includes the assembly bias of central and satellite galaxies, parameterized as  $Q_{\text{cen}}$  and  $Q_{\text{sat}}$ , respectively, to predict a suite of one- and two-point observables. In particular, our fiducial constraint employs the probability distribution of the galaxy number counts measured on  $8 \text{ Mpc } h^{-1}$  scales  $N_8^g$  and the projected cross-correlation functions of quintiles of galaxies selected by  $N_8^g$  with our entire galaxy sample. We perform extensive tests of the efficacy of our method by fitting the same observables to mock data using both constrained and non-constrained simulations. We discover that in many cases the level of cosmic variance between the two simulations can produce biased constraints that lead to an erroneous detection of galaxy assembly bias if the non-constrained simulation is used. When applying our method to the SDSS data, the ELUCID reconstruction effectively removes an otherwise strong degeneracy between cosmic variance and galaxy assembly bias in SDSS, enabling us to derive an accurate and stringent constraint on the latter. Our fiducial ELUCID constraint, for galaxies above a stellar mass threshold  $M_* = 10^{10.2} h^{-2} M_\odot$ , is  $Q_{\text{cen}} = -0.09 \pm 0.05$  and  $Q_{\text{sat}} = 0.09 \pm 0.10$ , indicating no evidence for a significant ( $> 2\sigma$ ) galaxy assembly bias in the local Universe probed by SDSS. Finally, our method provides a promising path to the robust modelling of the galaxy-halo connection within future surveys like DESI and PFS.

**spatial distribution of galaxies, large scale structure of the Universe, Numerical simulation**

**PACS number(s):** 98.62.Py, 98.65.Dx, 02.60.Cb

**Citation:** Salcedo A. N., Zu Y., Zhang Y., et al., Elucidating Galaxy Assembly Bias in SDSS, *Sci. China-Phys. Mech. Astron.* **60**, 000000 (2022), doi: 10.1007/s11432-016-0037-0

## 1 Introduction

As one of the most successful models of the galaxy-halo connection [89], the halo occupation distribution (HOD)

provides a convenient yet precise analytic framework for interpreting modern galaxy surveys (e.g. [8, 20, 21, 41, 50, 54, 55, 65, 72, 73, 82, 97, 108, 109]). In its simplest form, the standard HOD model assumes that the galaxy oc-

cupation inside dark matter haloes depends solely on halo mass. The physical basis for this assumption can be traced back to early theories of structure formation (e.g. [5, 10, 12, 44, 59, 67, 74]) in which the gravitational collapse and spatial clustering of dark matter halos are determined by the peak height in the initial density field. Since then, various numerical studies have robustly detected the so-called “halo assembly bias” effect using cosmological N-body simulations — halo clustering also depends on halo properties (e.g., concentration, formation time, spin, etc.) other than the mass (e.g. [27, 30, 31, 36, 42, 43, 52, 56, 68, 71, 75, 86, 90, 95]). If galaxy occupation inside haloes of the same mass varies with respect to a secondary halo property that manifests strong halo assembly bias the resulting “galaxy assembly bias” will make the clustering predictions of a standard HOD model inaccurate; HOD prescriptions and other models of the galaxy-halo connection would need to be modified accordingly. The potential existence of galaxy assembly bias is thus an important source of systematic uncertainty in cosmological interpretation of current and future galaxy surveys [22, 57, 113]. In this paper, we extend the standard HOD prescription to include both central and satellite assembly biases, and we constrain the level of galaxy assembly bias in the local Universe observed by the Sloan Digital Sky Survey (SDSS) using a novel combination of one and two-point statistics.

Observationally, many studies have attempted to detect galaxy assembly bias directly from SDSS, but the results so far are inconclusive or even in contradiction with one another. Using the SDSS Main Galaxy Sample, Zentner et al. [106] constrained galaxy assembly bias by fitting the galaxy clustering of different volume-limited galaxy samples with the galaxy assembly bias prescription of Hearin et al. [39]. They found that the  $M_r < -20$  sample favors non-zero central assembly bias at roughly the  $3\sigma$  level, while the  $M_r < -19$  sample favors non-zero satellite assembly bias at a weaker level. Focusing on the central galaxies of SDSS groups [100], Lin et al. [53] found little difference between the large-scale clustering of early and late-forming central galaxies that reside in haloes of the same weak lensing mass (but see [98]). However, applying a similar detection philosophy to the more massive luminous red galaxy sample in the SDSS-III Baryon Oscillation Spectroscopic Survey (BOSS; [23]), Niemiec et al. [62] claimed that the galaxies exhibit significant large-scale clustering discrepancies when divided into two subsamples based on stellar age [60].

Aside from galaxy clustering, the observed large-scale correlation of galaxy colours<sup>1)</sup>(a.k.a “galactic conformity” [46]) had been regarded as potential evidence of galaxy assembly bias [38]. However, Zu and Mandelbaum [111] found that the HOD framework of [109] can successfully explain the large-scale galactic conformity phenomenon, by combining the environmental dependence of the halo mass function [26, 51, 101, 107] and the halo mass quenching model [110], without any need for galaxy assembly bias. Other studies have reached similar conclusions with different methods [14, 76, 81]. Furthermore, Alam et al. [3] studied the dependence of galaxy clustering on density and geometric environment within SDSS. They found that the same HOD+halo quenching model can also reproduce the colour-dependent clustering of galaxies selected by large-scale overdensity as well as tidal anisotropy, which N-body studies show to be one of the most important drivers of halo assembly bias [64]. Therefore, any galaxy assembly bias effect appears to be weak in comparison to the environmental dependence of the halo mass function, which can be fully accounted for in the standard HOD.

Since the SDSS Main Galaxy Sample probes a relatively small volume ( $\sim(650 h^{-1}\text{Mpc})^3$ ; [104]) with a significant presence of cosmic variance in the large-scale structures [17], at least some of the inconsistencies among various detection results may arise from the fact that the cosmic variance in the halo clustering could be misinterpreted as evidence for galaxy assembly bias. In this paper, we mitigate such confusion by utilizing ELUCID, a state-of-the-art constrained simulation that accurately reconstructs the initial density perturbations of the SDSS volume. ELUCID provides a high-fidelity input halo catalogue that faithfully reproduces the large-scale environment of each *individual* halo in SDSS, effectively removing the impact of cosmic variance on our analysis.

Despite the lack of strong observational evidence of galaxy assembly bias, a wide variety of models have been proposed to extend traditional methods of galaxy-halo connection to allow different forms of its existence, from the “age-matching model” that introduced maximum correlation between galaxy colours and halo formation time [37], to the modifications to subhalo abundance matching proposed by Contreras et al. [18], to various proposed modifications to the HOD that introduce a secondary dependence of the occupation on a halo internal property at fixed halo mass [39, 102]. Alternatively, many studies have looked for insights on galaxy

1) For the small scale counterpart to this effect see [91].

assembly bias from hydrodynamic simulations and semi-analytic models, but its behavior differs among models depending on the exact details of the galaxy formation recipe [4, 7, 11, 16, 19, 35, 88, 94, 96, 103]. Instead of choosing a specific halo internal property as our proxy for galaxy assembly bias, following Wibking et al. [92] we adopt a more general/agnostic approach by parameterising central and satellite assembly biases as the variation of their halo occupation with the dark matter overdensity defined within a radius of  $8.0 h^{-1} \text{ Mpc}$  (see also [58, 69, 94]).

To further enhance our constraining power, in addition to the commonly used galaxy two-point correlation function  $w_p(r_p)$ , we also include the probability density distribution of large-scale galaxy number counts  $p(N_8^g)$ . Wang et al. [87] showed that the combination of one and two-point galaxy statistics can greatly improve on constraints from two-point statistics alone. Therefore, we anticipate that by combining correlation functions with galaxy observables that incorporate the one-point large-scale galaxy number count  $N_8^g$  we can produce more stringent constraints on galaxy assembly bias. Inspired by Abbas and Sheth [2], we also employ the galaxy number count dependent correlation functions  $w_p(r_p|N_8^g)$ , in hopes of extracting overdensity-dependent HODs in an analogous fashion to deriving global HOD parameters from the overall galaxy clustering.

The paper is organised as follows. In the next section we describe the data and simulations we use. In particular, section 2.1 describes the SDSS-DR7 stellar mass limited galaxy catalog, while section 2.2 describes the Bolshoi and ELUCID simulations and the methods of halo identification applied to both simulations to produce halo catalogs. Section 3 provides a detailed description of our HOD modelling methodology, including our extensions to the HOD to model galaxy assembly bias. Section 4 describes the galaxy clustering statistics we utilize in our analysis. Section 5 details the methods of our Markov chain Monte Carlo (MCMC) analysis. We present the results of fitting our data vectors to mock galaxy catalogs and SDSS data in sections 6 and 7 respectively. We summarize our results in section 8.

## 2 Data and Simulations

### 2.1 SDSS Main Galaxy Sample

We make use of the final data release of the SDSS I/II [1], which contains the completed data set of the SDSS-I and

SDSS-II. In particular, we employ the Main Galaxy Sample [79] data from the dr72 large-scale structure sample bright0 of the ‘New York University Value Added Catalogue’ (NYU-VAGC), constructed as described in Blanton et al. [9]. We apply the ‘nearest-neighbour’ scheme to correct for the 7% of galaxies that are without redshifts due to fibre collisions, and use data exclusively within the contiguous area in the North Galactic Cap and regions with angular completeness greater than 0.8.

We employ the stellar mass estimates from the latest MPA/JHU value added galaxy catalogue<sup>2)</sup>. The stellar masses were estimated based on fits to the SDSS photometry following the methods of Kauffmann et al. [45] and Salim et al. [70], and assuming the Chabrier [15] Initial Mass Function (IMF) and the Bruzual and Charlot [13] Stellar Population Synthesis (SPS) model.

We select all the SDSS galaxies within the redshift range  $z = [0.01, 0.09]$  and with stellar mass above  $M_*^{\text{min}} = 10^{10.2} h^{-2} M_\odot$ , yielding a sample of 82,824 galaxies in total. Based on the stellar mass completeness limit estimated by Zu and Mandelbaum [109], we believe this cut in redshift produces a galaxy sample that is roughly volume complete down to  $M_*^{\text{min}}$ . The volume of the resulting sample is  $\sim (230 h^{-1} \text{ Mpc})^3$ . Note that by extending the maximum redshift of our sample to 0.09, we will include the ‘Sloan Great Wall’ [33, SGW] at  $z \sim 0.08$  in our analysis. As one of the densest regions within the SDSS volume, galaxies in the SGW could potentially reveal the strongest galaxy assembly bias signal within our sample.

### 2.2 Simulations: ELUCID vs. Bolshoi

One of the key ingredients of our fiducial model is the constrained simulation ELUCID [85], which is a  $500^3 h^{-3} \text{ Mpc}^3$  cubic box containing  $3072^3$  particles with a particle mass of  $3.088 \times 10^8 h^{-1} M_\odot$ . The ELUCID cosmology is based on the results of the WMAP5 [25, 48]: a flat Universe with  $\Omega_\kappa = 0$ ,  $\Omega_{m,0} = 0.258$ ,  $\Omega_{\Lambda,0} = 0.742$ ,  $h = 0.72$ ,  $n_s = 0.96$ , and  $\sigma_8 = 0.80$ . Below we will briefly describe the ELUCID reconstruction, and refer to Wang et al. [84] for technical details of the method.

The ELUCID simulation reconstructs the density field of the nearby Universe using the SDSS DR7 group catalog of Yang et al. [100]<sup>3)</sup> and the Hamiltonian Markov Chain (HMC) Monte Carlo with Particle Mesh (PM) dynamics algorithm of Wang et al. [84]. The reconstruction was performed between  $z=0.01$  and 0.12, where the group catalog is roughly volume-complete above  $M_{\text{H}}=10^{12} h^{-1} M_\odot$ . Following Wang et al. [83], the red-

2) <https://home.strw.leidenuniv.nl/~jarle/SDSS/>

3) For a detailed description of the group finding algorithm see [99].

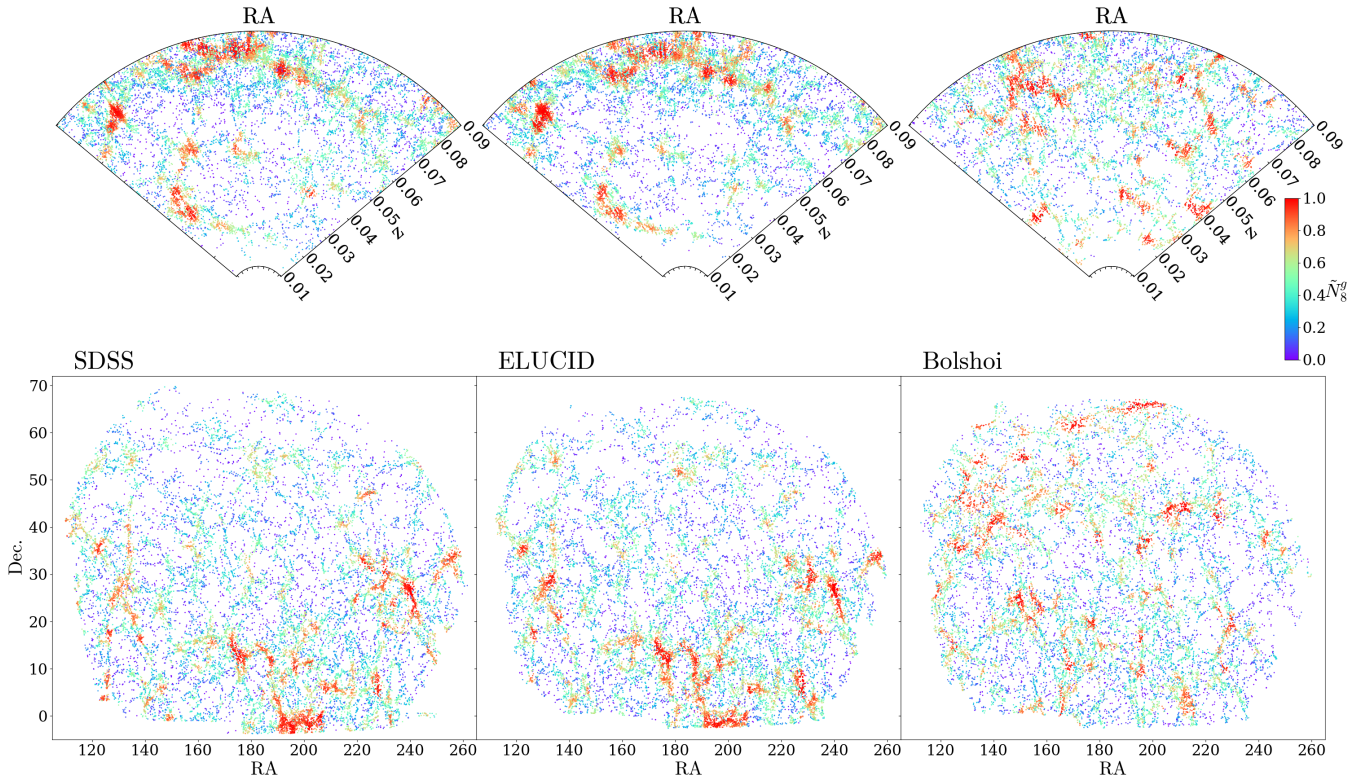


**Figure 1** Redshift wedges (top,  $\text{Dec} < 10.0^\circ$ ) and redshift slices (bottom,  $z = 0.08 - 0.09$ ) in SDSS (left), ELUCID (middle), and Bolshoi (right). Points represent the positions of galaxies, colored by their rank in the galaxy number count  $\bar{N}_g^g$  (described in 4.2). The striking similarity between SDSS and ELUCID demonstrates the efficacy of reconstruction in ELUCID, in sharp contrast with Bolshoi, which is a random realization of  $\Lambda\text{CDM}$ .

shift space distortions were statistically removed to estimate the real space distances to the groups. To reconstruct the present-day dark matter density field from the galaxy groups, ELUCID employed a halo-domain reconstruction method which partitions the local volume into a set of domains such that each domain contains exactly one halo and every point within the domain is closer to its halo than to any other using the distance metric  $r/R_h$  where  $R_h$  is the virial radius of the domain halo. Subsequently, pre-computed simulated halo-matter profiles are used to produce a density profile within each domain based on the mass of the domain halo. Finally, the HMC+PM method of Wang et al. [84] is applied to this present-day density field to reconstruct the initial density field at  $z_{\text{ini}} = 100$ , which is then evolved to  $z = 0$  using L-GADGET, a memory optimized version of GADGET-2 [78].

To compare to our fiducial results from ELUCID, we also use the publicly available Bolshoi-Planck simulation [47],<sup>4)</sup> which is a  $250^3 h^{-3} \text{Mpc}^3$  cubic box with  $2048^3$  particles, each  $1.350 \times 10^8 h^{-1} M_\odot$  in mass. The Bolshoi-Planck cosmology is based off of Planck 2016

[66], with  $\Omega_\kappa = 0$ ,  $\Omega_{m,0} = 0.3071$ ,  $\Omega_{\Lambda,0} = 0.6929$ ,  $h = 0.70$ ,  $n_s = 0.96$ , and  $\sigma_8 = 0.82$ . We will refer to this simulation simply as “Bolshoi” for the rest of the paper. For both simulations, we use the spherical overdensity halo catalogues produced by the standard Rockstar halo finder [6]. Our halo mass is defined so that the average density enclosed within the halo radius is 200 times the mean background density of the Universe.

Despite the slight differences in cosmology and mass resolution, we emphasize that the most important difference between these two simulations is the density reconstruction — ELUCID provides a dark matter density field that faithfully reproduces the large-scale environment of each *individual* group-sized halo observed in SDSS while Bolshoi does not. Therefore, any difference in the constraints on the galaxy-halo connection obtained using the two simulations should be driven primarily by cosmic variance, i.e., by the difference between structure in the SDSS volume modeled by ELUCID and the random realization of a periodic cube in Bolshoi. By comparing results from Bolshoi and ELUCID we are able to determine the extent to which cosmic variance

4) <https://www.cosmosim.org/cms/simulations/bolshoip/>

can bias constraints and potentially produce erroneous detections of galaxy assembly bias.

Figure 1 illustrates the effectiveness of the ELUCID reconstruction. Each panel shows the distribution of galaxies color-coded by a measurement of their large-scale galaxy number count  $N_8^g$  (described in detail in § 4.2), with red points existing in the most dense regions and purple in the least dense regions. The left panels show the distribution of the SDSS galaxies in our sample, while the middle panels show the distribution of mock galaxies within the SDSS-constrained region of ELUCID (note that this volume is not exactly the same as in data), generated using the best-fitting parameters of our fiducial constraint. The right panels show the distribution of Bolshoi mock galaxies populated using the same parameters as used for ELUCID. The visual similarities between the SDSS and ELUCID panels are striking, indicating that the ELUCID reconstruction, combined with our best-fitting HOD parameters, provides a high-fidelity galaxy density field that closely mimics the SDSS observation. While the ELUCID reconstruction is not perfect, especially in the low density regions where few groups above  $M_h=10^{12}h^{-1}M_\odot$  exist, the cosmic variance effect should be greatly reduced in the intermediate and high-density regions where the signal-to-noise of our measurements is the highest. In contrast, the Bolshoi simulation exhibits a typical large-scale structure pattern formed in  $\Lambda$ CDM, but it clearly fails to capture the most prominent structures in SDSS (e.g., the SGW). Naively, one might think that the Bolshoi simulation is adequate for constraining galaxy assembly bias if the galaxy sample is cut off at  $z = 0.075$  to avoid the SGW. However, the strong cosmic variance effect cannot be mitigated by deliberately removing the SGW from our analysis using Bolshoi, which could still produce a biased constraint on galaxy assembly bias due to the lack of high-density environments within the data.

### 3 Populating Simulations with Galaxies

We populate simulated haloes with mock galaxies according to an extended HOD framework. We will briefly describe the standard HOD component in § 3.1 and introduce our extension for incorporating galaxy assembly bias in § 3.2.

#### 3.1 Halo Occupation Distribution

Following the standard practice (e.g. [49, 104, 105, 108]), we separate galaxies into centrals and satellites, so that for a stellar mass-threshold sample haloes have an av-

erage probability  $\langle N_{\text{cen}}(M_h) \rangle$  of hosting a central and the mean satellite occupation  $\langle N_{\text{sat}}(M_h) \rangle$  is an increasing power law in mass. We parametrize the two mean galaxy occupation numbers of haloes as

$$\langle N_{\text{cen}}(M_h) \rangle = \frac{1}{2} \left[ 1 + \text{erf} \left( \frac{\log M_h - \log M_{\text{min}}}{\sigma_{\log M}} \right) \right], \quad (1)$$

$$\langle N_{\text{sat}}(M_h) \rangle = \langle N_{\text{cen}}(M_h) \rangle \left( \frac{M_h - M_0}{M_1} \right)^\alpha. \quad (2)$$

where  $M_{\text{min}}$  refers to the characteristic mass to host a central (i.e.  $\langle N_{\text{cen}}(M_h) = 0.5 \rangle$ ),  $\sigma_{\log M}$  is the width of the transition from  $\langle N_{\text{cen}} \rangle = 0.0$  to  $\langle N_{\text{cen}} \rangle = 1.0$ ,  $M_1$  is the normalization of the satellite-occupation power-law,  $M_0$  truncates the satellite power-law, and  $\alpha$  is the power-law index.

The number of centrals is sampled from a Bernoulli distribution. The number of satellites placed into an individual halo is sampled from a Poisson distribution centered on the mean satellite occupation. We place central galaxies at the minimum of the potential of their host haloes. Satellites are distributed according to a Navarro-Frenk-White (NFW; [61]) shape parametrized by halo concentration  $c_{200\text{m}} = r_{200\text{m}}/r_s$  and truncated at  $r_{200\text{m}}$  the halo radius that encloses average density equal to 200 times the mean background density of the Universe. We measure halo concentrations directly from the simulations and include an additional parameter  $\mathcal{A}_{\text{con}}$  to allow for the profiles of hosted satellite galaxies to differ from the dark matter profiles of their host haloes

$$c_{200\text{m}}^{\text{gal}} = \mathcal{A}_{\text{con}} \times c_{200\text{m}}^{\text{DM}}. \quad (3)$$

Finally, we include the effect of redshift space distortions in our mocks. In both ELUCID and Bolshoi we measure the dark matter three dimensional velocity dispersion of each of our halos  $\sigma_{\text{DM}}$ . We assign central and satellite velocities following the work of Guo et al. [34]. For each central galaxy, the velocity  $v_{\text{cen}}$  relative to that of its host halo is drawn from an exponential distribution,

$$p(v_{\text{cen}} - v_h) = \frac{1}{\sqrt{2}\sigma_{\text{DM}}} \exp \left( -\frac{\sqrt{2}|v_{\text{cen}} - v_h|}{\sigma_{\text{DM}}} \right), \quad (4)$$

where  $v_h$  is the relevant component of host halo velocity. For each satellite galaxy we draw the velocity components relative to that of the host from a Gaussian distribution with dispersion  $\sigma_{\text{DM}}$ . Guo et al. [34] include parameters to model central and satellite velocity bias, but since we have found these parameters to have very little effect on our observables we set them to zero and unity respectively. We displace the positions of our

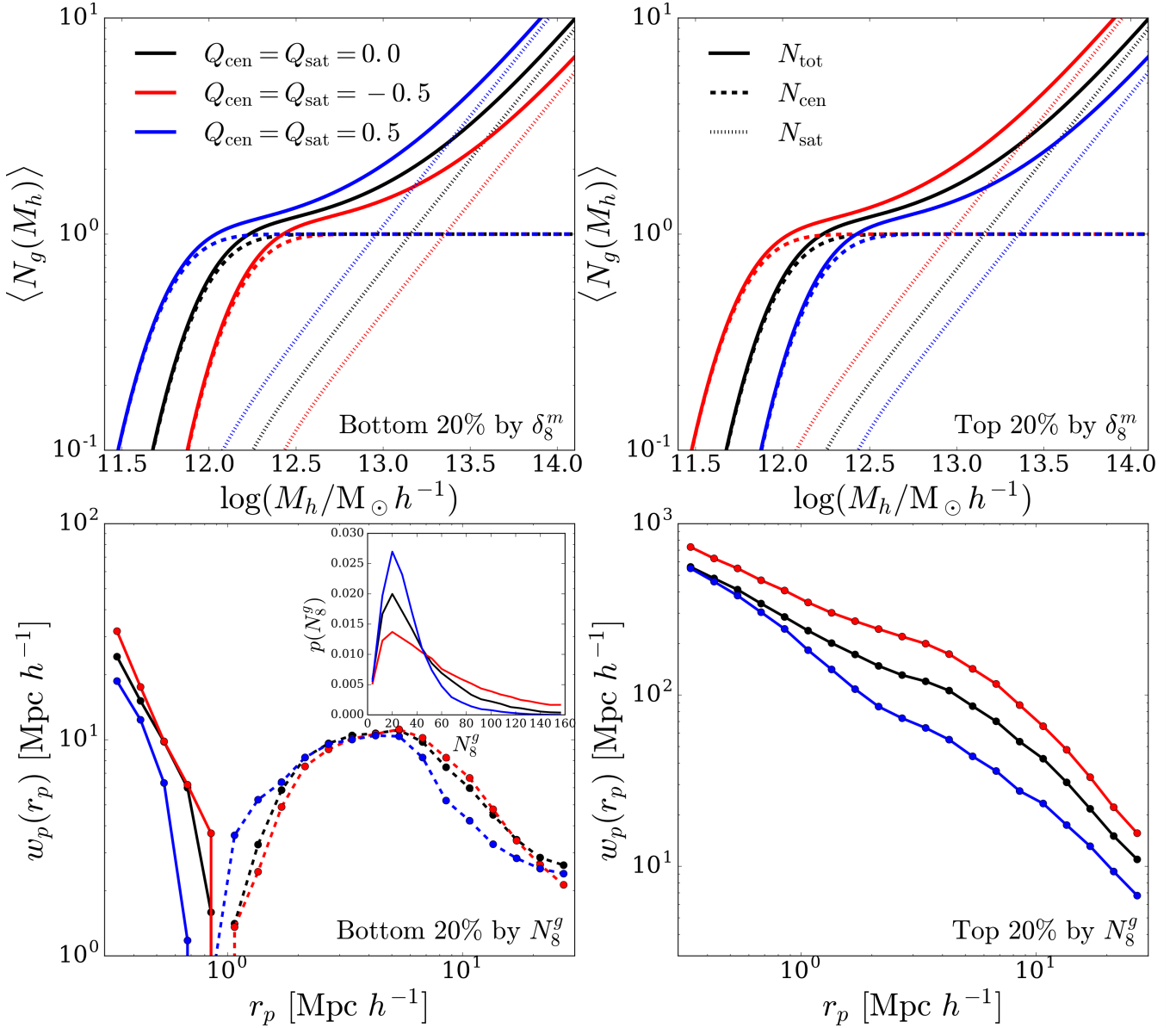


**Figure 2** Top panels: HODs of galaxies in the bottom ( $\delta_8^m < 0.20$ , left) and top ( $\delta_8^m > 0.80$ , right) quintiles of matter overdensity rank  $\delta_8^m$ , for three galaxy assembly bias models with  $Q_{\text{cen}}=Q_{\text{sat}}=0.0$  (black),  $Q_{\text{cen}}=Q_{\text{sat}}=-0.5$  (red), and  $Q_{\text{cen}}=Q_{\text{sat}}=0.5$  (blue), respectively. In both panels we show the total HOD (solid) along with central (dashed) and satellite (dotted) contributions. Bottom panels: Projected cross-correlation functions of the bottom (left) and top (right) galaxy quintiles of the galaxy number count rank  $N_8^g$  (described in § 4.2) with the global galaxy sample for the three models of galaxy assembly bias. In the bottom left panel the dashed lines correspond to negative values of the correlation function. Additionally we show the PDF of  $N_8^g$  in the inset of the bottom left panel for the three models.

mock galaxies using the line-of-sight components of the assigned velocities. In ELUCID we assume the position of the observer is at Earth, and in Bolshoi we adopt the z-axis as the line-of-sight direction.

### 3.2 Modeling Galaxy Assembly Bias

For the purpose of our analysis, galaxy assembly bias refers to the potential dependence of the galaxy occupation on properties other than halo mass. Properties

that are often considered in the literature include internal properties like halo formation time and concentration, but this definition does not exclude environmental properties such as the large scale overdensity or tidal anisotropy. When such a secondary property exhibits a halo assembly bias signal at fixed mass, the clustering of galaxies will be modified from the standard HOD prediction on both small and large scales. In particular, in the absence of galaxy assembly bias, the linear galaxy bias  $b_g(M_h)$  at fixed halo mass  $M_h$  is equal to the linear

halo bias  $b_h(M_h)$ . However, a galaxy assembly bias with respect to halo property  $x$  will introduce some covariance between  $N_{\text{gal}}(x|M_h)$  and  $b(x|M_h)$ , producing a linear galaxy bias  $b_g^x(M_h)$  that is modified from  $b_g(M_h)$

$$\begin{aligned} b_g^x(M_h) &= \sum_{i=0}^{N_h} N_{\text{gal}}(x_i | M_h) b(x_i | M_h) / \sum_{i=0}^{N_h} N_{\text{gal}}(x_i | M_h) \\ &= \langle N_{\text{gal}}(x | M_h) b(x | M_h) \rangle / \langle N_{\text{gal}}(M_h) \rangle \\ &= b_g(M_h) + \text{cov}(N_{\text{gal}}, b | M_h) / \langle N_{\text{gal}}(M_h) \rangle, \end{aligned} \quad (5)$$

where  $\text{cov}(N_{\text{gal}}, b | M_h)$  is the covariance between galaxy occupation  $N_{\text{gal}}(x, M_h)$  and  $b(x, M_h)$  at  $M_h$ , and  $\langle N_{\text{gal}}(M_h) \rangle$  is the average galaxy occupation at  $M_h$ . If we further assume the galaxy occupation follows the Poisson distribution, which is an accurate approximation for high-occupancy haloes, the extra term on the right can be expressed by

$$\begin{aligned} \Delta b_g &= b_g^x(M_h) - b_g(M_h) \\ &= \rho_{cc} \sigma(b | M_h) / \sqrt{\langle N_{\text{gal}}(M_h) \rangle}, \end{aligned} \quad (6)$$

where  $\rho_{cc}$  and  $\sigma(b | M_h)$  are the cross-correlation coefficient and the scatter in halo bias at  $M_h$ , respectively. On small scales, galaxy assembly bias will increase the second moment of the galaxy occupation  $\langle N_{\text{gal}}^2 | M_h \rangle$  while minimally affecting the mean occupation, thereby boosting galaxy clustering in the 1-halo regime by adding more satellite-satellite pairs [8].

It is unclear which halo internal property is most responsible for galaxy assembly bias if it exists. A variety of studies have examined galaxy assembly bias within hydrodynamic simulations and semi-analytic models and produced valuable insights (e.g. [4, 7, 11, 16, 19, 35, 88, 94, 96, 103]), but as of yet we lack a physical and observational understanding of galaxy assembly bias. Although halo formation time and concentration are some of the most commonly-used secondary variables for modeling galaxy assembly bias (e.g. [39, 87, 106]), there is no observational evidence suggesting that one variable is more physically-motivated than another. Therefore, we will take a more agnostic approach and look for a generic variable that is mathematically more convenient. According to Equation 6, we would want a variable that exhibits a very strong (anti-)correlation with halo bias, i.e.,  $|\rho_{cc}| \rightarrow 1$ . The obvious candidate variable is the halo bias itself defined on the basis of individual haloes, i.e., the large-scale dark matter overdensity. In particular, we implement a modified version of the parameterization of Wibking et al. [92] (see also [58, 69, 94]). Wibking et al. [92] allow  $M_{\text{min}}$  to vary on a halo-by-halo basis according to the large scale matter-overdensity measured

on  $8 \text{ Mpc } h^{-1}$  scales  $\delta_8^m$ . This environmental dependence is written as

$$\log M_{\text{min}} = \log M_{\text{min},0} + Q_{\text{cen}} (\tilde{\delta}_8^m - 0.5), \quad (7)$$

where  $Q_{\text{cen}}$  expresses the strength of the dependence of  $M_{\text{min}}$  on environment and  $\tilde{\delta}_8^m \in [0, 1]$  is the normalized rank of  $\delta_8^m$  within a narrow mass bin. Using the *rank* of  $\delta_8^m$  has the advantage of being less sensitive to the particular choice of  $8 \text{ Mpc } h^{-1}$ . When  $Q_{\text{cen}}$  is positive haloes in dense environments are less likely to host centrals, and vice versa when it is negative. The case of  $Q_{\text{cen}} = 0.0$  corresponds to having no assembly bias. Similar to Xu et al. [94] we extend this parameterization by allowing  $M_1$  to also vary according to environment,

$$\log M_1 = \log M_{1,0} + Q_{\text{sat}} (\tilde{\delta}_8^m - 0.5). \quad (8)$$

In the top two panels of Figure 2, we illustrate the effect of the two galaxy assembly bias parameters on the total (solid lines), central (dashed) and satellite (dotted) halo occupations for galaxies selected by their large scale matter overdensity  $\delta_8^m$ . We plot the predicted occupation for  $Q_{\text{cen}}=Q_{\text{sat}}=0.0$  (black lines),  $Q_{\text{cen}}=Q_{\text{sat}}=-0.5$  (red) and  $Q_{\text{cen}}=Q_{\text{sat}}=0.5$  (blue), respectively, while keeping all the other HOD parameters fixed. The top left panel shows variations of the HOD for galaxies in underdense environments while the top right panel shows variations for those in overdense environments. By design, when  $Q_{\text{cen}}=Q_{\text{sat}}=0$  there is no variation in HOD for different environments. However, when  $Q_{\text{cen}}=Q_{\text{sat}}=-0.5$  both  $M_{\text{min}}$  and  $M_1$  are increased (decreased) in underdense (overdense) environments. This has the effect of boosting the galaxy occupation of haloes of a given mass that are in overdense environments. When  $Q_{\text{cen}}=Q_{\text{sat}}=0.5$  we observe the opposite behavior, with both  $M_{\text{min}}$  and  $M_1$  decreased (increased) in underdense (overdense environments).

## 4 Observables

### 4.1 Galaxy Clustering

We compute the projected galaxy correlation functions  $w_p$  by integrating the real-space correlation function along the line of sight

$$w_p(r_p) = 2 \int_0^{\Pi_{\text{max}}} \xi(r_p, \pi) d\pi, \quad (9)$$

where  $r_p$  and  $\pi$  are the projected pair separation and the line-of-sight distance, respectively, and  $\xi$  is the real-space isotropic correlation function. We compute  $\xi$  with

the Natural estimator

$$\xi(r) = \frac{DD(r)}{RR(r)} - 1, \quad (10)$$

where  $DD(r)$  and  $RR(r)$  are the number of galaxy-galaxy and random-random pairs with pair separation  $r$ , respectively. When computing  $w_p$  in the ELUCID and SDSS volumes we compute the random-random term using random catalogs constructed with the same geometry as ELUCID and SDSS respectively. When computing  $w_p$  in Bolshoi we analytically compute the random-random term as  $RR=2\pi\Pi_{\max}(r_{p,\max}^2-r_{p,\min}^2)(N_g^2/L_{\text{box}}^3)$ .

We choose to set the integration limit  $\Pi_{\max} = 30 h^{-1} \text{Mpc}$ . This value is chosen to balance the need to have a large enough  $\Pi_{\max}$  to mitigate the uncertainties in our modelling of the redshift-space distortions and to suppress noise arising from uncorrelated structure along the line of sight. We calculate  $\xi(r_p, \pi)$  using CORRFUNC [77] in 20 logarithmically-spaced bins from  $r_{p,\min}=0.3 h^{-1} \text{Mpc}$  to  $r_{p,\max}=30.0 h^{-1} \text{Mpc}$  and in  $1.0 h^{-1} \text{Mpc}$ -wide bins in  $\pi$ , respectively.

## 4.2 Galaxy Number Counts

To enhance the constraining power of our HOD model with ELUCID, we supplement the two-point galaxy statistic  $w_p$  with a one-point statistic — the probability density distribution (PDF) of galaxy number counts measured on  $8 \text{Mpc} h^{-1}$  scales around each galaxy  $N_g^g$ . When computing  $N_g^g$  for galaxies in the SDSS-constrained volume of ELUCID we include neighbour galaxies outside of the SDSS-constrained volume. Although this technically means our measurement of  $N_g^g$  in ELUCID includes contributions from non-constrained regions, the number of galaxies affected is small.

Motivated by the results of Abbas and Sheth [2] and Alam et al. [3], we use the quantity  $N_g^g$  to define count-selected subsamples of galaxies and compute their clustering statistics. Specifically, we divide our galaxies into quintiles of  $N_g^g$  and compute their projected cross-correlation functions with the global sample. We denote these correlation functions as  $w_p(r_p|\tilde{N}_g^{g,i})$ , where  $\tilde{N}_g^{g,i}$  refers to the  $i$ -th quintile selected by  $N_g^g$ . In addition to the global clustering  $w_p$  and the probability distribution of galaxy overdensity  $p(N_g^g)$  we use these count-selected quintile cross-correlation functions to constrain assembly bias. We anticipate that the clustering of the most extreme over/underdense regions should be particularly sensitive to galaxy assembly bias because it is in those regions that the HOD is most significantly modified from the standard form if galaxy assembly bias exists (see equations 7 and 8).

## 4.3 Impact of Galaxy Assembly Bias on Observables

The bottom two panels of Figure 2 illustrate the effects of the galaxy assembly bias parameters on our observables. The bottom left panel shows the variation among the cross-correlation functions between the global sample and the bottom 20% of galaxies selected by  $N_g^g$  as predicted by the three galaxy assembly bias models shown in the top left panel. Similarly, the bottom right panel shows the cross-correlation variation for the top 20% of galaxies selected by  $N_g^g$ , with their HODs shown in the top right panel. In both sets of panels, black lines show results for  $Q_{\text{cen}}=Q_{\text{sat}}=0.0$  (i.e., zero galaxy assembly bias), red lines show results for  $Q_{\text{cen}}=Q_{\text{sat}}=-0.5$ , and blue lines for  $Q_{\text{cen}}=Q_{\text{sat}}=0.5$ . In each case we keep all other HOD parameters fixed. Note that these variations in  $Q_{\text{cen}}$  and  $Q_{\text{sat}}$  are exaggerated compared to the values allowed by the data for illustrative purposes. We also show the effects of assembly bias on the PDF of galaxy number count  $p(N_g^g)$  in the inset of the bottom left panel.

For the galaxies in the bottom quintile of  $N_g^g$ , the correlation functions are negative at large scales and we plot the amplitude of these negative values with dashed lines. On small scales, the cross-correlation effectively measures the 1-halo term of the typical host halo. For the  $Q_{\text{cen}}=Q_{\text{sat}}=0.5$  case, the galaxies on average live in haloes of much lower mass than those in the  $Q_{\text{cen}}=Q_{\text{sat}}=-0.5$  case, producing a significantly lower clustering on scales below  $3 h^{-1} \text{Mpc}$ . On large scales, the  $Q_{\text{cen}}=Q_{\text{sat}}=0.5$  case exhibits a stronger cross-correlation (i.e., less negative). This is consistent with the inset panel where the average  $N_g^g$  of the bottom quintile in the  $Q_{\text{cen}}=Q_{\text{sat}}=0.5$  case is higher than the other two, because the model places more galaxies in low-density regions.

The effects of  $Q_{\text{cen}}$  and  $Q_{\text{sat}}$  on the clustering of the highest galaxy quintile selected by  $N_g^g$  are shown in the bottom right panel of Figure 2. In the case of  $Q_{\text{cen}}=Q_{\text{sat}}=-0.5$ , the clustering of galaxies in the top  $N_g^g$ -quintile is boosted at all scales. At large scales this is because the occupation of haloes in overdense environments has been boosted. On small scales, since haloes that host galaxies in high- $N_g^g$  environments are generally more massive, and the number of satellite pairs at fixed halo mass is higher compared to the zero-assembly-bias mock, the galaxy clustering is also strongly boosted. For the  $Q_{\text{cen}}=Q_{\text{sat}}=0.5$  galaxies, the clustering signal decreases at all scales relative to  $Q_{\text{cen}}=Q_{\text{sat}}=0.0$ . However, the difference is the least significant at the smallest scales of  $r_p$ . This is because at these small scales the effect of positive  $Q_{\text{sat}}$  on  $\langle N_{\text{gal}}^2 | M \rangle$  also acts to boost the number of satellite pairs, which compensates for the im-



pect from having a lower average halo occupation in dense regions. At large scales the clustering is influenced only by the latter effect, and therefore the effect of setting  $Q_{\text{sat}}=Q_{\text{cen}}=0.5$  is opposite in sign to that of setting  $Q_{\text{sat}}=Q_{\text{cen}}=-0.5$ , albeit with similar amplitude.

Galaxy assembly bias also modifies the relative fraction of the low vs. high overdensity environments, by shifting the galaxy population into halos in low or high density regions. The inset of the bottom left panel of Figure 2 shows such effects on the PDF of  $N_8^g$  from setting non-zero values of  $Q_{\text{cen}}$  and  $Q_{\text{sat}}$ . When  $Q_{\text{cen}}=Q_{\text{sat}}=-0.5$  the PDF is broadened with the density increasing at large values of  $N_8^g$  relative to the PDF for  $Q_{\text{cen}}=Q_{\text{sat}}=0.0$ . This increase is driven by the fact that negative values of  $Q_{\text{cen}}$  and  $Q_{\text{sat}}$  cause highly clustered haloes to have higher occupations which increases the overall values of  $N_8^g$ . This effect is mitigated however by the fact that the PDF has an explicit integral constraint. The effect of setting  $Q_{\text{cen}}=Q_{\text{sat}}=0.5$  on the halo occupation is the opposite, causing less clustered haloes to have higher occupations for their mass. This causes the PDF to narrow and decreases the number of galaxies with high  $N_8^g$ .

To summarize, Figure 2 demonstrates that, in the absence of other systematic uncertainties, the combination of the PDF of  $N_8^g$  and the cross-correlation functions of galaxies selected by  $N_8^g$  is a very sensitive probe of galaxy assembly bias. Any deviation of  $Q_{\text{cen}}$  and  $Q_{\text{sat}}$  from zero will generate coherent variation in the HOD between high and low density regions of the Universe. This galaxy assembly bias effect in the HOD, coupled with the environmental modulation of the halo mass function, produces a unique set of phenomena in the overdensity distribution and density-dependent cross-correlation functions that can potentially be detected within the SDSS data.

#### 4.4 Distinguishing Cosmic Variance and Galaxy Assembly Bias

Cosmic variance can also significantly affect the measurements of one and two-point statistics in the SDSS volume, including the stellar mass function [17] and the two-point correlation function of the faint red galaxies [93]. Therefore, a slight tendency of SDSS galaxies to reside in high (low) density regions due to cosmic variance could be misinterpreted as evidence for negative (positive) values of  $Q_{\text{cen}}$  and  $Q_{\text{sat}}$ .

To mitigate the confusion due to cosmic variance, we utilize the ELUCID constrained simulation as an input to our fiducial HOD analysis. As shown in Figure 1,

ELUCID reproduces most of the specific structure observed in the local SDSS volume, in sharp contrast with the Bolshoi simulation that does not. Because Bolshoi and ELUCID have reasonably similar cosmologies this difference is primarily driven by cosmic variance. It is possible for this cosmic variance to bias constraints on assembly bias (or other HOD parameters) obtained from fitting our galaxy observables. This is particularly the case for the  $N_8^g$ -selected correlation functions, because they are very sensitive to the extremely low or high-density structures. For example, Zehavi et al. [104] identified that the Sloan Great Wall is the most significant cosmic variance effect on their measurements of the global  $w_p$ , and we thus expect a much stronger impact on the  $w_p$  of galaxies in the top quintile of  $N_8^g$ .

Figure 3 shows a more quantitative comparison of the cosmic variance and galaxy assembly bias effects on the five  $N_8^g$ -selected correlation functions. Circles with errorbars are the measurements from a mock galaxy sample constructed using ELUCID without galaxy assembly bias. Using this measurement as our mock observables, we derive constraints  $Q_{\text{cen}} = -0.15^{+0.06}_{-0.06}$  and  $Q_{\text{sat}} = 0.18^{+0.17}_{-0.15}$  with our extended HOD model using the Bolshoi simulation. The solid lines are the predictions from the best-fitting model with  $Q_{\text{cen}} = -0.15$  and  $Q_{\text{sat}} = 0.18$ . As a consistency check, dotted lines indicate the prediction from the best-fitting HOD model that uses ELUCID haloes as input (a fit that favors no assembly bias by recovering the true values of  $Q_{\text{cen}}=Q_{\text{sat}}=0.0$ ). Clearly, the Bolshoi best-fit does a very poor job describing the  $w_p$  of galaxies in the top (red) and bottom (purple) quintiles, largely due to cosmic variance between Bolshoi and ELUCID. However, once we apply the Bolshoi best-fit as is directly to the ELUCID haloes, the predictions, indicated by the dashed lines, provide a reasonably good description of the data points without any fitting. The significant reduction of  $\chi^2$  from 82.10 to 49.09 suggests that the cosmic variance effect is the main hurdle to obtaining a satisfactory goodness of fit for the HOD model, especially for galaxies in the highest density regions. Because of cosmic variance, the Bolshoi fit spuriously favors a non-zero value of  $Q_{\text{cen}}$  at  $2.5\sigma$  significance, and even with the freedom allowed by assembly bias it cannot achieve a good match to the data. The ELUCID mock with incorrect parameters reproduces the data better but is nonetheless distinguishable at high significance from the correct model.

One can argue that instead of describing the Bolshoi fit results as biased, we should simply say that our observational errors are under-estimated. To overcome such

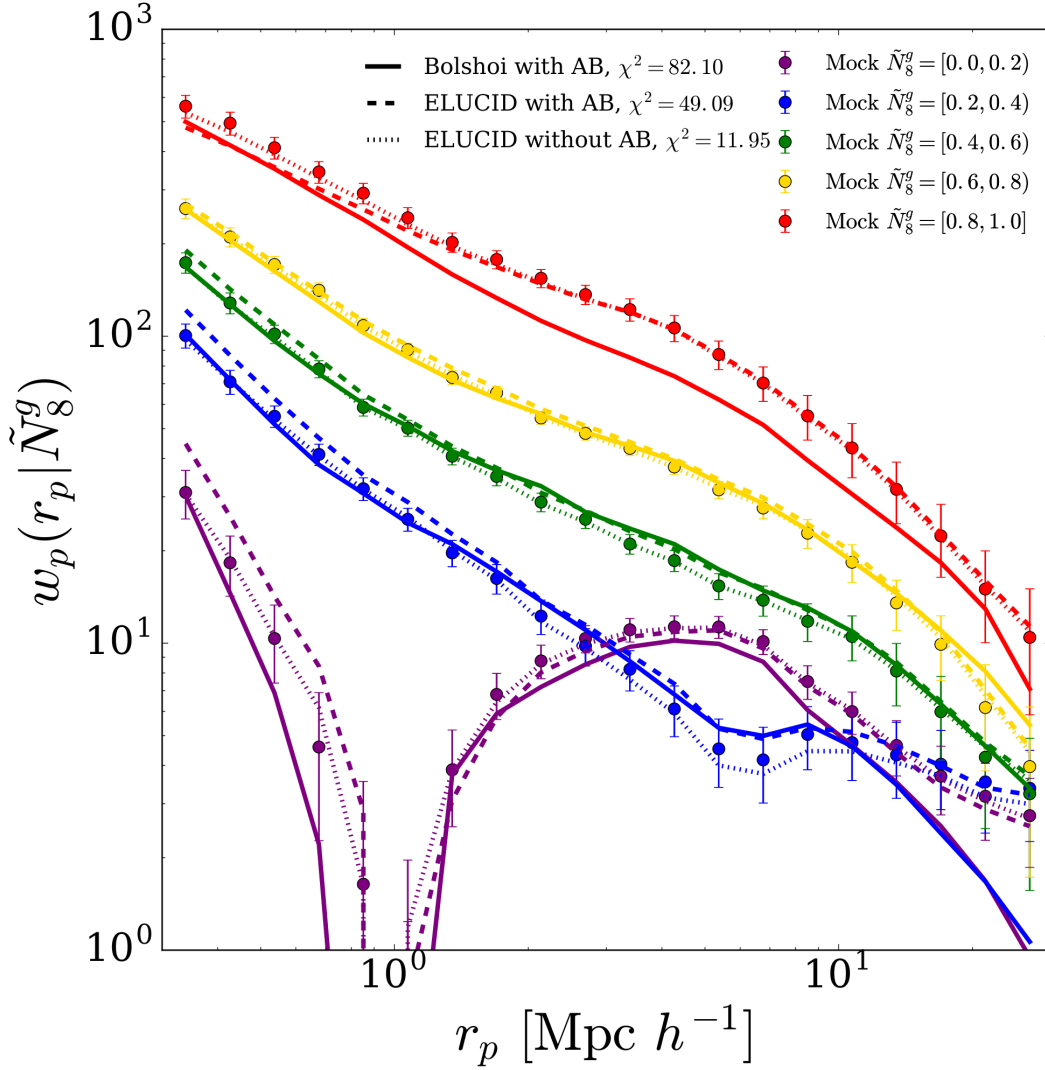


**Figure 3** Impact of cosmic variance on the projected cross-correlation functions between mock galaxies in number count  $N_8^g$  quintiles and the global galaxy sample. Circles with errorbars show the measurements from an ELUCID galaxy mock built without galaxy assembly bias, while dotted lines show the results of a consistency test of fitting to this ELUCID galaxy mock using ELUCID halos ( $\chi^2=11.95$ ). Solid lines show the predictions from the best-fitting HOD model inferred from fitting to the mock data (circles) using Bolshoi halos, which results in a false detection of galaxy assembly bias with  $Q_{\text{cen}}=-0.15$  and  $Q_{\text{sat}}=0.18$ . Dashed lines show the results of directly applying the same HOD with non-zero values of  $Q_{\text{cen}}$  and  $Q_{\text{sat}}$  to ELUCID halos without any fitting. The false detection, along with the significant improvement in the goodness of fit from the solid ( $\chi^2=82.10$ ) to the dashed lines ( $\chi^2=49.09$ ), illustrates the vital importance of mitigating cosmic variance when constraining galaxy assembly bias.

shortcoming, we can either compute the covariance matrix from a large number of simulations with different initial conditions, or base our analysis on a constrained simulation like ELUCID that faithfully reproduces the large-scale structure in the SDSS volume. However, the former approach is computationally prohibitive, while the latter approach, which we adopt in this paper, has the added benefit that we can estimate the covariance matrix via jackknife re-sampling of the data (see §Appendix A), as is commonly done by similar analyses in the literature, whether it be HOD modelling or detecting galaxy assembly bias.

## 5 Gaussian Likelihood Model

In both our mock tests and our data constraints we consider four different combinatorial data vectors,

1. The combination of projected galaxy two-point function and galaxy number density  $\{w_p(r_p), n_g\}$ .
2. The combination of projected galaxy two-point function, PDF of galaxy overdensity, and galaxy number density  $\{w_p(r_p), p(N_8^g), n_g\}$ .
3. The cross-correlation functions between galaxies in quintiles of  $N_8^g$  and the global sample, and the

galaxy number density  $\{w_p(r_p|\tilde{N}_8^{g,i})|_{i=1-5}, n_g\}$ .

4. The cross-correlation functions between galaxies in quintiles of  $N_8^g$  and the global sample, the PDF of galaxy overdensity, and the galaxy number density  $\{w_p(r_p|\tilde{N}_8^{g,i})|_{i=1-5}, p(N_8^g), n_g\}$ . This is our fiducial data vector.

To constrain HOD and galaxy assembly bias parameters we fit to these four data vectors measured from either SDSS galaxies or mock galaxies constructed using ELUCID haloes. In each case we use the appropriate covariance matrix described in Appendix A and assume 5% Gaussian errors on  $n_g$ , uncorrelated with errors in other observables. We assume a Gaussian likelihood model,  $\mathcal{L} \propto e^{-\chi^2/2}$ , where

$$\chi^2 = \frac{(n_g^{\text{mock}} - n_g)^2}{(0.05 \times n_g)^2} + \sum_{i,j} \Delta\mathcal{D}(x_i) [C^{-1}]_{ij} \Delta\mathcal{D}(x_j), \quad (11)$$

where  $C^{-1}$  is the inverse covariance matrix and  $\Delta\mathcal{D}(x_i) \equiv \mathcal{D}^{\text{mock}}(x_i) - \mathcal{D}(x_i)$  is the difference between mock and measured data vector  $\mathcal{D}$ . We measure  $w_p$ , and  $w_p(r_p|\tilde{N}_8^{g,i})|_{i=1-5}$  in 20 logarithmically spaced bins from 0.3 to  $30.0 h^{-1} \text{ Mpc}$  with  $\Pi_{\text{max}}=30.0 h^{-1} \text{ Mpc}$ . We measure  $p(N_8^g)$  in 20 linearly spaced bins from  $N_8^g=0.0$  to  $N_8^g=160.0$ . When measuring any of our data vectors in ELUCID we only use galaxies within the SDSS constrained volume and within redshift range  $0.01 \leq z \leq 0.09$ . This choice is made to match to the volume of our SDSS data sample. When using Bolshoi we use the entire volume of the cubic box.

We infer posterior parameter distributions for our model parameters by performing Markov Chain Monte Carlo (MCMC) sampling using the parallel affine-invariant ensemble sampler of Goodman and Weare [32] implemented in the EMCEE python module [28]. In all cases we use 1000 walkers and remove the first  $10^5$  burn-in samples.

<sup>5)</sup> A value of  $|Q_{\text{cen}}|=2.0$ , for instance, would mean that the effective value of  $M_{\text{min}}$  could vary by an entire order of magnitude at fixed mass based on large scale overdensity.

**Table 1** Parameter priors used in our likelihood analysis and input values of HOD parameters to our two ELUCID galaxy mocks, one built without galaxy assembly bias (Mock A) and the other with strong galaxy assembly bias (Mock B).

| Parameter                   | Prior                       | Mock A | Mock B |
|-----------------------------|-----------------------------|--------|--------|
| $\sigma_{\log M}$           | [0.01, 0.80]                | 0.20   | 0.20   |
| $\log M_{\text{min}}$       | [11.0, 12.5]                | 11.95  | 11.95  |
| $\log M_1$                  | [12.0, 13.5]                | 13.15  | 13.15  |
| $\alpha$                    | [0.6, 2.0]                  | 1.0    | 1.0    |
| $\mathcal{A}_{\text{con.}}$ | $\mathcal{N}(0.86, 0.12^2)$ | 0.86   | 0.86   |
| $Q_{\text{cen}}$            | [-2.0, 2.0]                 | 0.0    | -0.5   |
| $Q_{\text{sat}}$            | [-2.0, 2.0]                 | 0.0    | +0.5   |

We have found that the parameter  $M_0$  has negligible effect on all of our observables and is poorly constrained; we therefore fix  $\log M_0=11.40$  in all cases. We also adopt a Gaussian prior on  $\mathcal{A}_{\text{con.}}$  centered at  $\mathcal{A}_{\text{con.}}=0.86$  with standard deviation 0.12. This prior is motivated by the results of Zu et al. [112] who applied an HOD analysis to the clustering and lensing data for the same SDSS-DR7 catalog that we use. For all other parameters we adopt uniform priors listed in Table 1. In all such cases our priors are non-informative. Although our galaxy assembly bias parameters can technically assume values in the range  $(-\infty, \infty)$  the priors we impose upon them are non-informative and cover all physically plausible values of the two parameters.<sup>5)</sup>

## 6 Model Tests Using ELUCID Mock Galaxies

Before analysing data from SDSS, we perform a variety of mock tests that will be described below. In addition to allowing us to confirm the robustness of our method, these mock tests compare the relative precision of different data vectors, and investigate the level of systematic bias in parameter estimation due to cosmic variance. The values of the HOD parameters used to populate the two mocks, one with zero and the other with strong galaxy assembly bias, are listed in Table 1.

We select the values of input HOD parameters for our mock with no galaxy assembly bias (Mock A) that produce reasonably good agreement with our observables measured in SDSS, and only change the values of  $Q_{\text{cen}}$  and  $Q_{\text{sat}}$  while keeping the other parameters fixed for our mock with strong galaxy assembly bias (Mock B). In what follows we will refer to our HOD analysis as “fitting ELUCID or Bolshoi haloes to ELUCID or SDSS

**Table 2** Posterior constraints of model parameters from the ELUCID mock with no galaxy assembly bias. The column ‘Haloos’ refers to the simulation used to compute the likelihood. Values quoted are posterior modes with 68% confidence intervals. The value of  $\chi^2/\text{d.o.f}$  is calculated from the mean of the posterior samples. Input values are listed in the last row.

| Data vector  | Haloos  | $\sigma_{\log M}$      | $\log M_{\min}$         | $\log M_1$              | $\alpha$               | $\mathcal{Q}_{\text{cen}}$ | $\mathcal{Q}_{\text{sat}}$ | $\mathcal{A}_{\text{con.}}$ | $\chi^2/\text{d.o.f}$ |
|--|---------|------------------------|-------------------------|-------------------------|------------------------|----------------------------|----------------------------|-----------------------------|-----------------------|
| $\{w_p(r_p), n_g\}$                                      | ELUCID  | $0.34^{+0.30}_{-0.23}$ | $12.00^{+0.12}_{-0.07}$ | $13.19^{+0.17}_{-0.13}$ | $0.97^{+0.14}_{-0.11}$ | $-0.01^{+0.22}_{-0.30}$    | $-0.04^{+0.70}_{-0.58}$    | $0.85^{+0.12}_{-0.12}$      | 2.01/14               |
| $\{w_p(r_p), n_g\}$                                      | Bolshoi | $0.38^{+0.29}_{-0.26}$ | $11.99^{+0.12}_{-0.09}$ | $13.09^{+0.21}_{-0.16}$ | $0.88^{+0.10}_{-0.10}$ | $-0.05^{+0.21}_{-0.40}$    | $-0.59^{+1.10}_{-0.81}$    | $0.85^{+0.12}_{-0.12}$      | 7.33/14               |
| $\{w_p(r_p), p(N_8^g), n_g\}$                            | ELUCID  | $0.20^{+0.05}_{-0.05}$ | $11.95^{+0.03}_{-0.02}$ | $13.14^{+0.05}_{-0.06}$ | $0.96^{+0.05}_{-0.06}$ | $0.00^{+0.06}_{-0.06}$     | $0.01^{+0.09}_{-0.09}$     | $0.81^{+0.09}_{-0.08}$      | 6.68/34               |
| $\{w_p(r_p), p(N_8^g), n_g\}$                            | Bolshoi | $0.19^{+0.09}_{-0.09}$ | $11.89^{+0.03}_{-0.03}$ | $13.11^{+0.07}_{-0.08}$ | $0.99^{+0.07}_{-0.07}$ | $0.04^{+0.07}_{-0.06}$     | $-0.20^{+0.11}_{-0.12}$    | $0.83^{+0.12}_{-0.10}$      | 44.92/34              |
| $\{w_p(r_p \tilde{N}_8^{g,i}) _{i=1-5}, n_g\}$           | ELUCID  | $0.17^{+0.09}_{-0.09}$ | $11.94^{+0.03}_{-0.03}$ | $13.14^{+0.06}_{-0.05}$ | $0.98^{+0.05}_{-0.05}$ | $-0.02^{+0.06}_{-0.05}$    | $0.03^{+0.12}_{-0.10}$     | $0.83^{+0.10}_{-0.10}$      | 11.96/94              |
| $\{w_p(r_p \tilde{N}_8^{g,i}) _{i=1-5}, n_g\}$           | Bolshoi | $0.20^{+0.10}_{-0.11}$ | $11.94^{+0.04}_{-0.03}$ | $13.01^{+0.08}_{-0.08}$ | $0.89^{+0.04}_{-0.05}$ | $-0.15^{+0.06}_{-0.06}$    | $0.18^{+0.17}_{-0.15}$     | $0.79^{+0.10}_{-0.13}$      | 81.48/94              |
| $\{w_p(r_p \tilde{N}_8^{g,i}) _{i=1-5}, p(N_8^g), n_g\}$ | ELUCID  | $0.20^{+0.04}_{-0.04}$ | $11.95^{+0.02}_{-0.02}$ | $13.15^{+0.04}_{-0.04}$ | $0.96^{+0.04}_{-0.04}$ | $0.00^{+0.05}_{-0.04}$     | $0.01^{+0.07}_{-0.07}$     | $0.80^{+0.07}_{-0.06}$      | 18.72/114             |
| $\{w_p(r_p \tilde{N}_8^{g,i}) _{i=1-5}, p(N_8^g), n_g\}$ | Bolshoi | $0.19^{+0.05}_{-0.06}$ | $11.92^{+0.02}_{-0.02}$ | $13.09^{+0.04}_{-0.06}$ | $0.96^{+0.04}_{-0.05}$ | $0.02^{+0.05}_{-0.05}$     | $-0.06^{+0.10}_{-0.12}$    | $0.79^{+0.09}_{-0.10}$      | 120.53/114            |
| Input Value  | -       | 0.20                   | 11.95                   | 13.15                   | 1.0                    | 0.0                        | 0.0                        | 0.86                        | -                     |

**Table 3** Similar to Table 2 but for the mock with significant level of galaxy assembly bias.

| Data vector  | Haloos  | $\sigma_{\log M}$      | $\log M_{\min}$         | $\log M_1$              | $\alpha$               | $\mathcal{Q}_{\text{cen}}$ | $\mathcal{Q}_{\text{sat}}$ | $\mathcal{A}_{\text{con.}}$ | $\chi^2/\text{d.o.f}$ |
|--|---------|------------------------|-------------------------|-------------------------|------------------------|----------------------------|----------------------------|-----------------------------|-----------------------|
| $\{w_p(r_p), n_g\}$                                      | ELUCID  | $0.32^{+0.30}_{-0.22}$ | $12.00^{+0.12}_{-0.07}$ | $13.18^{+0.17}_{-0.14}$ | $0.97^{+0.11}_{-0.10}$ | $-0.58^{+0.25}_{-0.19}$    | $0.67^{+0.64}_{-0.55}$     | $0.86^{+0.12}_{-0.12}$      | 1.23/14               |
| $\{w_p(r_p), n_g\}$                                      | Bolshoi | $0.45^{+0.26}_{-0.31}$ | $12.01^{+0.11}_{-0.10}$ | $13.05^{+0.18}_{-0.15}$ | $0.91^{+0.11}_{-0.10}$ | $-0.51^{+0.32}_{-0.40}$    | $-0.03^{+1.14}_{-0.82}$    | $0.86^{+0.12}_{-0.12}$      | 7.07/14               |
| $\{w_p(r_p), p(N_8^g), n_g\}$                            | ELUCID  | $0.20^{+0.07}_{-0.07}$ | $11.96^{+0.04}_{-0.03}$ | $13.14^{+0.07}_{-0.07}$ | $0.97^{+0.06}_{-0.06}$ | $-0.50^{+0.05}_{-0.05}$    | $0.50^{+0.08}_{-0.08}$     | $0.82^{+0.12}_{-0.11}$      | 3.53/34               |
| $\{w_p(r_p), p(N_8^g), n_g\}$                            | Bolshoi | $0.13^{+0.11}_{-0.08}$ | $11.90^{+0.05}_{-0.04}$ | $12.91^{+0.11}_{-0.10}$ | $0.88^{+0.08}_{-0.07}$ | $-0.26^{+0.08}_{-0.09}$    | $0.01^{+0.17}_{-0.13}$     | $0.85^{+0.12}_{-0.11}$      | 33.34/34              |
| $\{w_p(r_p \tilde{N}_8^{g,i}) _{i=1-5}, n_g\}$           | ELUCID  | $0.17^{+0.10}_{-0.09}$ | $11.94^{+0.03}_{-0.03}$ | $13.12^{+0.09}_{-0.09}$ | $0.99^{+0.05}_{-0.05}$ | $-0.51^{+0.06}_{-0.06}$    | $0.50^{+0.18}_{-0.15}$     | $0.88^{+0.11}_{-0.11}$      | 11.53/94              |
| $\{w_p(r_p \tilde{N}_8^{g,i}) _{i=1-5}, n_g\}$           | Bolshoi | $0.20^{+0.09}_{-0.08}$ | $11.93^{+0.04}_{-0.03}$ | $13.01^{+0.07}_{-0.07}$ | $0.92^{+0.04}_{-0.04}$ | $-0.50^{+0.07}_{-0.08}$    | $0.41^{+0.21}_{-0.15}$     | $0.81^{+0.12}_{-0.12}$      | 72.73/94              |
| $\{w_p(r_p \tilde{N}_8^{g,i}) _{i=1-5}, p(N_8^g), n_g\}$ | ELUCID  | $0.20^{+0.04}_{-0.05}$ | $11.95^{+0.02}_{-0.02}$ | $13.15^{+0.04}_{-0.04}$ | $0.98^{+0.04}_{-0.04}$ | $-0.50^{+0.03}_{-0.04}$    | $0.50^{+0.05}_{-0.05}$     | $0.81^{+0.08}_{-0.08}$      | 14.71/114             |
| $\{w_p(r_p \tilde{N}_8^{g,i}) _{i=1-5}, p(N_8^g), n_g\}$ | Bolshoi | $0.18^{+0.06}_{-0.07}$ | $11.91^{+0.03}_{-0.02}$ | $12.96^{+0.06}_{-0.06}$ | $0.92^{+0.04}_{-0.04}$ | $-0.37^{+0.06}_{-0.07}$    | $0.17^{+0.17}_{-0.11}$     | $0.76^{+0.12}_{-0.12}$      | 109.19/114            |
| Input Value  | -       | 0.20                   | 11.95                   | 13.15                   | 1.0                    | -0.50                      | 0.50                       | 0.86                        | -                     |

galaxies”. By this we mean that we populate ELUCID or Bolshoi haloos with our HOD prescription to compute model likelihoods to fit to data vectors calculated using either ELUCID mock galaxies or SDSS galaxies. For each of the four data vectors, we perform four separate mock tests, two by fitting ELUCID haloos to ELUCID mock galaxies constructed with and without galaxy assembly bias, and the other two by fitting Bolshoi haloos to the same ELUCID mock galaxies. The results of our 16 mock constraints from this section are listed in Table 2 using Mock A and Table 3 using Mock B; values quoted correspond to parameter posterior modes and 68% confidence intervals. The results of an analogous set of tests for Mock B, but with the values of  $\mathcal{Q}_{\text{cen}}$  and  $\mathcal{Q}_{\text{sat}}$  kept fixed to zero, can be found in Appendix B.

### 6.0.1 The $\{w_p(r_p), n_g\}$ Data Vector

All the standard HOD parameters listed in Table 2 and 3 are correctly recovered in all four cases, albeit sometimes with large uncertainties (especially  $\sigma_{\log M}$ ) or dominated by priors (e.g.,  $\mathcal{A}_{\text{con.}}$ ). In each case, the constraint is statistics-limited, so that the cosmic variance between ELUCID and Bolshoi is not discernible in either the goodness of fit or the size of the uncertainties. For all four cases, the marginalized 1D constraints on  $\mathcal{Q}_{\text{cen}}$  and  $\mathcal{Q}_{\text{sat}}$  are consistent with the input, but the very large uncertainties render the constraint largely useless.

The marginalized 2D joint constraints in the  $\mathcal{Q}_{\text{cen}}$  vs.  $\mathcal{Q}_{\text{sat}}$  plane are highlighted in Figure 4 as yellow contours in each panel. A strong degeneracy of anti-correlation between the two parameters emerges in the 2D constraints, and in the Bolshoi case the degeneracy drives a  $\sim 1.5\sigma$  deviation from the true values of  $\mathcal{Q}_{\text{sat}}$  and

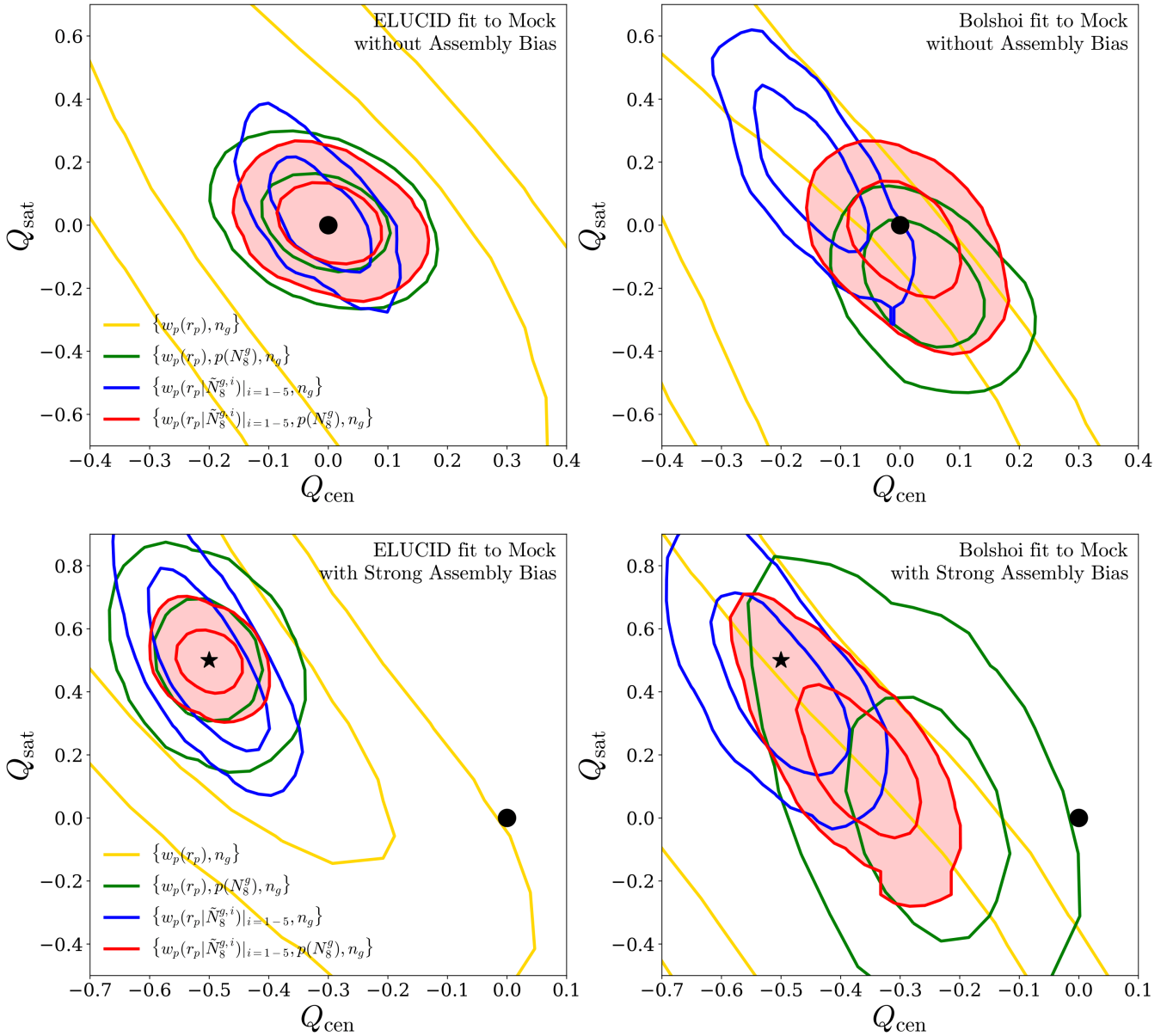


**Figure 4** Posterior constraints on  $Q_{\text{cen}}$  and  $Q_{\text{sat}}$  from fitting either ELUCID (left) or Bolshoi (right) haloes to the ELUCID mock with (bottom) or without (top) assembly bias. In each panel, we show the 68% and 95% confidence regions derived from using the  $\{w_p(r_p), n_g\}$  (yellow),  $\{w_p(r_p), p(N_8^g), n_g\}$  (green),  $\{w_p(r_p | R_\delta^i)_{i=1-5}, n_g\}$  (blue), and  $\{w_p(r_p | R_\delta^i)_{i=1-5}, p(N_8^g), n_g\}$  (red) data vectors, respectively. The black circle marks  $Q_{\text{cen}}=Q_{\text{sat}}=0.0$ , while the black star marks the input values for populating the ELUCID galaxy mock with strong galaxy assembly bias. Red shading highlights our fiducial choice of data vector.

$Q_{\text{cen}}$  (black circle and star in the top and bottom panels, respectively). The degeneracy track is unsurprising, as a change in  $Q_{\text{cen}}$  can always be partially compensated by a change of  $Q_{\text{sat}}$  of the opposite sign. The deviation, however, is either a result of the slight difference in cosmology or of cosmic variance. We consider it unlikely that this difference is caused by cosmology for two reasons. Firstly, the actual difference in cosmological parameters

between the two simulations is reasonably small (e.g.,  $\sigma_8=0.80$  vs.  $0.82$ ) relative to the expected sensitivity of  $w_p$  on these parameters<sup>6</sup>). Secondly, if the discrepancy were attributable to cosmology we would expect that our other HOD parameters would be similarly affected if not more so. Unlike our four traditional HOD parameters, both  $Q_{\text{cen}}$  and  $Q_{\text{sat}}$  act to decouple the one and two-halo scales, and they also introduce a unique scale depen-

6) See, for example, figure 4 of [69].

dence to the correlation function. Therefore, we believe that any discrepancy between the ELUCID and Bolshoi constraints is primarily driven by the cosmic variance as observed in Figure 1.

Overall, we find that  $\{w_p(r_p), n_g\}$  is not very effective at constraining galaxy assembly bias for an SDSS-like sample, but it provides the baseline constraints that we will compare to when examining the constraints from more advanced data vectors below.

### 6.0.2 The $\{w_p(r_p), p(N_8^g), n_g\}$ Data Vector

We now turn to mock tests performed with the  $\{w_p(r_p), p(N_8^g), n_g\}$  data vector. Compared to the  $\{w_p(r_p), n_g\}$  tests, adding  $p(N_8^g)$  produces drastically improved the precision of the constraints. Our constraint on  $\sigma_{\log M}$  has sharpened to 25%, an improvement of a factor of five. Similarly the constraints on the parameters  $\log M_{\min}$  and  $\log M_1$  have sharpened considerably by a factor of about three, while the constraint on  $\alpha$  has also improved by a factor of 2-3.

Focusing on our galaxy assembly bias parameters  $Q_{\text{cen}}$  and  $Q_{\text{sat}}$ , Figure 4 shows their constraints in green contours in each panel. The  $\{w_p(r_p), p(N_8^g), n_g\}$  data vector also significantly improves the precision of the constraints in all cases, but the inclusion of  $p(N_8^g)$  tends to shift the constraints towards the high- $Q_{\text{cen}}$ , low- $Q_{\text{sat}}$  direction in the Bolshoi fits (right panels). For Mock A with zero galaxy assembly bias, the 2D joint constraint is still consistent with the input at  $\sim 1\sigma$  (top right panel), but the shift produces a much stronger bias ( $>2\sigma$ ) for Mock B when the input is far from  $Q_{\text{sat}} = Q_{\text{cen}} = 0$  (bottom right panel). In the two left panels when ELUCID haloes are used, the  $\{w_p(r_p), p(N_8^g), n_g\}$  data vector yields constraints that are not only tightened but also stay unbiased.

Therefore, despite the difference of detail between  $p(N_8^g)$  and the count-in-cell statistics used by Wang et al. [87], we confirm their finding that by combining one and two-point statistics one can obtain an improved constraint on galaxy assembly bias, but with the caveat that the impact of cosmic variance is greatly mitigated.

### 6.0.3 The $\{w_p(r_p|\tilde{N}_8^{g,i})|_{i=1-5}, n_g\}$ Data Vector

Next we examine mock tests performed with the  $\{w_p(r_p|\tilde{N}_8^{g,i})|_{i=1-5}, n_g\}$  data vector. Overall, the 1D constraints on the standard HOD parameters are very similar compared to those using  $\{w_p(r_p), p(N_8^g), n_g\}$ , suggesting that the constraining power on the global HOD is comparable between  $w_p(r_p) + p(N_8^g)$  and  $w_p(r_p|\tilde{N}_8^{g,i})|_{i=1-5}$ .

This is unsurprising because the combination of five count-dependent correlation functions should contain all the information encoded in the global  $w_p(r_p)$  and some of the key information on the shape of the galaxy number count distribution.

In the left panels of Figure 4), the constraints derived using  $\{w_p(r_p|\tilde{N}_8^{g,i})|_{i=1-5}, n_g\}$  (blue contours) also exhibit similar levels of accuracy compared to those using  $\{w_p(r_p), p(N_8^g), n_g\}$  (green contours), with the input values of  $Q_{\text{cen}}$  and  $Q_{\text{sat}}$  correctly recovered regardless of having zero (top left) or strong (bottom left) galaxy assembly bias. When the Bolshoi haloes are used (right panels), however, the constraints using  $w_p(r_p|\tilde{N}_8^{g,i})|_{i=1-5}, n_g$  shift to the low- $Q_{\text{cen}}$ , high- $Q_{\text{sat}}$  regime, in the opposite direction compared to the shift caused by including  $p(N_8^g)$  (green contours). This shift produces a  $\sim 2\sigma$  bias in the  $Q_{\text{cen}}-Q_{\text{sat}}$  plane when there is no galaxy assembly bias (top right), but stays within  $1\sigma$  when the galaxy assembly bias is strong (bottom right).

Combining the test results from using  $\{w_p(r_p), p(N_8^g), n_g\}$  (green contours) and  $\{w_p(r_p|\tilde{N}_8^{g,i})|_{i=1-5}, n_g\}$  (blue contours), we find that although each data vector can produce biased constraints at the  $2\sigma$  level in the presence of strong cosmic variance,  $p(N_8^g)$  and  $w_p(r_p|\tilde{N}_8^{g,i})|_{i=1-5}$  shift the constraint in the opposite direction with each other. This behavior indicates that the galaxy assembly bias information present in the two observables are relatively independent, and by combining the two (i.e. our fiducial data vector below) we can potentially break some of the degeneracy between galaxy assembly bias and cosmic variance.

### 6.0.4 The $\{w_p(r_p|\tilde{N}_8^{g,i})|_{i=1-5}, p(N_8^g), n_g\}$ Data Vector

Finally, we examine the mock tests performed with  $\{w_p(r_p|\tilde{N}_8^{g,i})|_{i=1-5}, p(N_8^g), n_g\}$ , the input data vector that will be adopted for our fiducial constraint when analysing the SDSS data. In general, the constraints on the standard HOD parameters are marginally improved compared to the  $\{w_p(r_p|\tilde{N}_8^{g,i})|_{i=1-5}, n_g\}$  case, except for  $\sigma_{\log M}$ , for which the constraint improves by about a factor of two.

More important, this data vector provides more robust constraints on the galaxy assembly bias parameters. For the ELUCID fit to Mock A (top left), the derived constraint is  $Q_{\text{cen}} = -0.00_{-0.04}^{+0.05}$  and  $Q_{\text{sat}} = 0.01_{-0.07}^{+0.07}$ , in excellent agreement with the input values. For the Bolshoi fit to Mock A (top right), adding  $p(N_8^g)$  brings the constraints significantly closer to the input values compared to the large discrepancy observed when only  $\{w_p(r_p|\tilde{N}_8^{g,i})|_{i=1-5}, n_g\}$  is used, from  $Q_{\text{cen}} = -0.15_{-0.06}^{+0.06}$

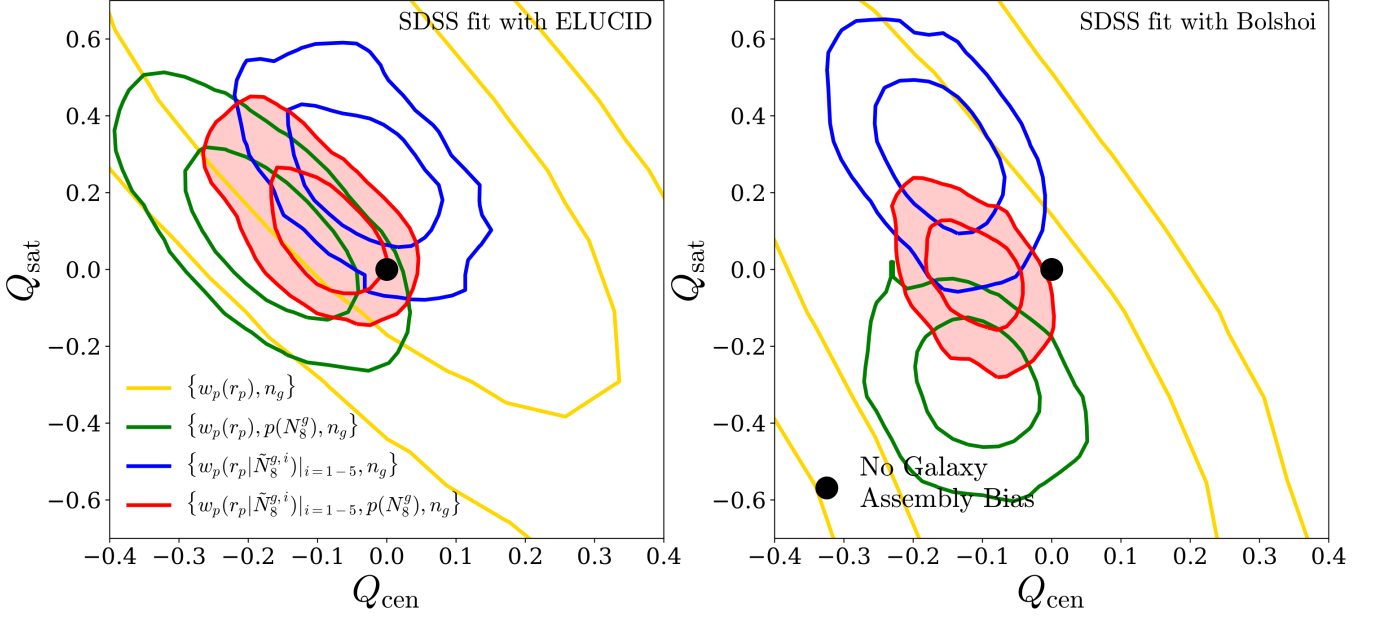


**Figure 5** Similar to Figure 4 but for constraints from the SDSS galaxies, with black circles indicating  $Q_{\text{cen}}=Q_{\text{sat}}=0.0$  as a visual reference to the case of no assembly bias. Red shading highlights the constraint from our fiducial choice of data vector.

and  $Q_{\text{sat}}=0.18^{+0.17}_{-0.15}$ , a  $2\sigma$  deviation in this 2D space, to  $Q_{\text{cen}}=0.02^{+0.05}_{-0.05}$  and  $Q_{\text{sat}}=-0.06^{+0.10}_{-0.12}$  (i.e., within  $1\sigma$  deviation). This improvement is reassuring — the residual cosmic variance between ELUCID and SDSS should be much smaller than that between Bolshoi and ELUCID, so we expect the amount of bias in our constraints on  $Q_{\text{cen}}$  and  $Q_{\text{sat}}$  to be significantly smaller than the statistical uncertainties. Meanwhile, the fits to Mock B exhibit similar results, except that the deviation increases in the Bolshoi fit (bottom right) but still within  $2\sigma$ .

To summarize, through a variety of mock tests with ELUCID and Bolshoi haloes, we find that our galaxy assembly bias constraints from the  $\{w_p(r_p), n_g\}$ ,  $\{w_p(r_p), p(N_g^g), n_g\}$  and,  $\{w_p(r_p) | \tilde{N}_8^{g,i} |_{i=1-5}, n_g\}$  data vectors are sensitive to the impact of cosmic variance. In contrast, the constraints from the  $\{w_p(r_p) | \tilde{N}_8^{g,i} |_{i=1-5}, p(N_g^g), n_g\}$  data vector are largely unbiased, despite the strong level of cosmic variance between ELUCID and Bolshoi. Among the four data vectors,  $\{w_p(r_p) | \tilde{N}_8^{g,i} |_{i=1-5}, p(N_g^g), n_g\}$  also produces the most stringent constraints on the galaxy assembly bias parameters. Therefore, for our analysis of the real data, we will apply our extended HOD model to the ELUCID simulation to fit the  $\{w_p(r_p) | \tilde{N}_8^{g,i} |_{i=1-5}, p(N_g^g), n_g\}$  data vector measured from SDSS as our fiducial analysis.

## 7 Galaxy Assembly Bias Constraint from SDSS

Informed by the extensive mock tests conducted in § 6, we conclude that the  $\{w_p(r_p) | \tilde{N}_8^{g,i} |_{i=1-5}, p(N_g^g), n_g\}$  data vector is the optimal choice for the input measurements to our fiducial constraint. We nonetheless fit ELUCID and Bolshoi haloes to the SDSS data using all four data vectors listed in § 5. We summarize the results of the 1D constraints in Table 4 and show the 2D constraints for all the parameter pairs in Figure 6, respectively. Overall, the constraints derived from the SDSS galaxies are very similar to those in the mock tests from the ELUCID mock galaxies, in terms of both the precision using each data vector and the trends with data vectors/simulations.

The constraints on the galaxy assembly bias parameters are highlighted in the left (ELUCID) and right (Bolshoi) panels of Figure 5, with the red filled contours indicating the results from our fiducial data vector  $\{w_p(r_p) | \tilde{N}_8^{g,i} |_{i=1-5}, p(N_g^g), n_g\}$ . In each panel, yellow, green, and blue open contours represent the constraints from using  $\{w_p(r_p), n_g\}$ ,  $\{w_p(r_p), p(N_g^g), n_g\}$ , and  $\{w_p(r_p) | \tilde{N}_8^{g,i} |_{i=1-5}, n_g\}$ , respectively. Again, we observe similar behavior of each data vector using either simulation as in Figure 5. In particular, the  $\{w_p(r_p), n_g\}$  constraints are the weakest with strong degeneracy exhibited between  $Q_{\text{cen}}$  and  $Q_{\text{sat}}$ . Adding  $p(N_g^g)$  tightens the constraints significantly while bringing the con-

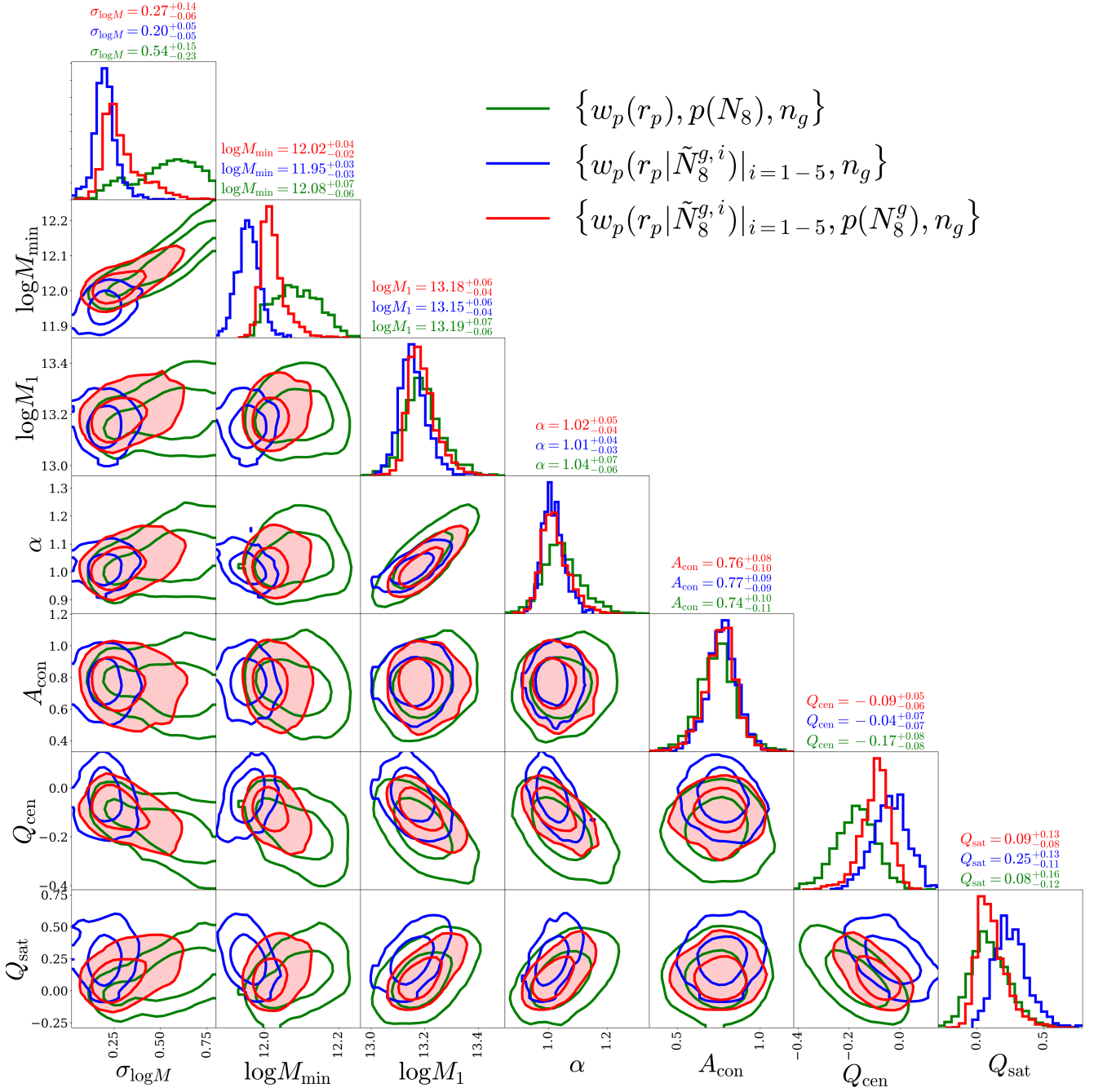


**Figure 6** Posterior constraints from our MCMC analysis of the SDSS data, derived from  $\{w_p(r_p), p(N_8^g), n_g\}$  (green),  $\{w_p(r_p | \tilde{N}_8^{g,i}) |_{i=1-5}, n_g\}$  (blue), and our fiducial data vector  $\{w_p(r_p | \tilde{N}_8^{g,i}) |_{i=1-5}, p(N_8^g), n_g\}$  (red filled contours and red histograms). Contours in each off-diagonal panel show the 68% and 95% confidence regions, and histograms in each diagonal panel show the 1D marginalized posterior distribution of each parameter, with values quoted above corresponding to the posterior mode and 68% confidence intervals.

tours into  $\sim 1.5\sigma$  tension with the zero values of  $Q_{\text{cen}}$  and  $Q_{\text{sat}}$ . Swapping  $w_p(r_p | \tilde{\delta}_8^{g,i}) |_{i=1-5}$  for  $p(N_8^g)$  further tightens the constraints, and exhibits similar deviation from  $Q_{\text{cen}}=Q_{\text{sat}}=0$  — the blue contours are inconsistent with zero galaxy assembly bias at the  $1.5\sigma$  (ELUCID) and  $> 2\sigma$  (Bolshoi) levels, respectively. However, because of the analogous but well-understood

behaviors shown in our high-fidelity mock tests, we can safely attribute the discrepancy largely to the (residual) cosmic variance between the simulations and SDSS. Finally, the fiducial ELUCID constraints with  $\{w_{p,gg}(r_p | \tilde{N}_8^{g,i}) |_{i=1-5}, p(N_8^g), n_g\}$  (red filled contours on the left panel) are consistent with  $Q_{\text{cen}} \equiv Q_{\text{sat}} = 0$  at  $1\sigma$ . Analogous constraints using Bolshoi (red filled contours on



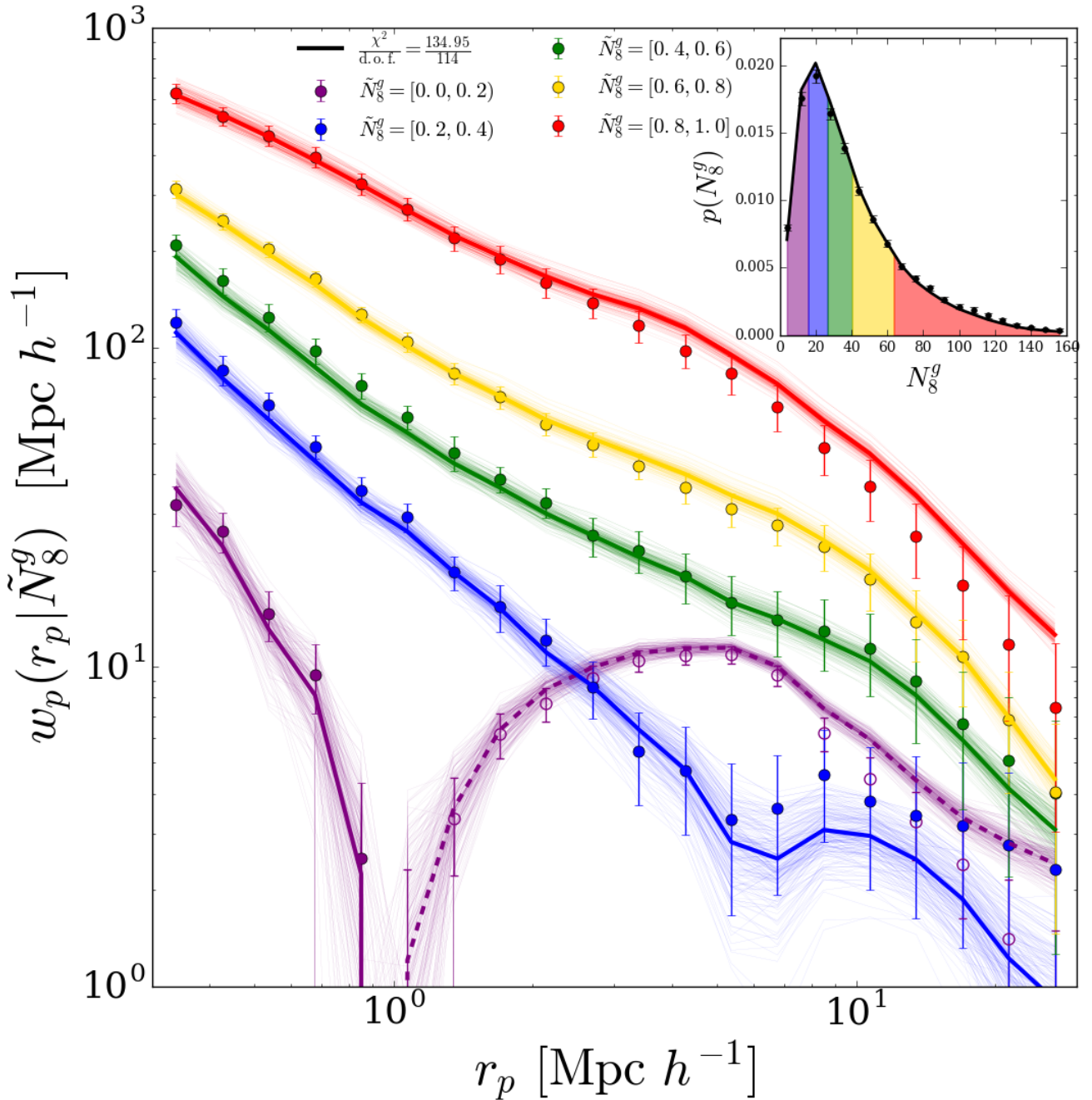


**Figure 7** Comparison of the measured projected cross-correlation functions between galaxy quintiles selected in  $N_8^g$  and the global galaxy sample (circles with errorbars) and those predicted by our posterior mean model with ELUCID (thick solid curves). Thin bundle of light-coloured curves surrounding each thick solid curve represent the predictions from 100 random steps along the MCMC chain of our SDSS analysis. The inset panel shows the data (black circles with errorbars) vs. model prediction (solid curve) comparison for  $p(\delta_8^g)$ , with the five filled vertical bands underneath the black curve indicating the quintiles in  $N_8^g$ . Note that the legend gives values of the rank quantity  $\tilde{N}_8^g$  not  $N_8^g$ . The posterior model produces a good description to the data with a  $\chi^2$  value of 134.95 for 114 degrees of freedom.

the right panel) are in  $2\sigma$  tension with  $Q_{\text{cen}}=Q_{\text{sat}}=0$  a difference attributable to the large cosmic variance between Bolshoi and SDSS.

Therefore, based on our fiducial SDSS analysis using the constrained simulation ELUCID, we obtain a stringent marginalized 1D constraint of  $Q_{\text{cen}} = -0.09^{+0.05}_{-0.06}$

and  $Q_{\text{sat}} = 0.09^{+0.13}_{-0.08}$ , hinting at a significant detection of galaxy assembly bias at above  $1\sigma$  level and close to  $2\sigma$  (at least for the centrals). However, the marginalized 2D constraint on the  $Q_{\text{cen}}-Q_{\text{sat}}$  plane (red contours on the left panel of Figure 5) is consistent with having no assembly bias at  $1\sigma$  and well within  $2\sigma$ . Given

**Table 4** Posterior constraints of model parameters from the SDSS data. The column ‘Haloed’ refers to the simulation used to compute the likelihood. Values quoted are posterior modes with 68% confidence intervals. The value of  $\chi^2/\text{d.o.f}$  is calculated from the mean of the posterior samples.

| Data vector  | Haloed  | $\sigma_{\log M}$      | $\log M_{\min}$         | $\log M_1$              | $\alpha$               | $Q_{\text{cen}}$        | $Q_{\text{sat}}$        | $\mathcal{A}_{\text{con.}}$ | $\chi^2/\text{d.o.f}$ |
|--|---------|------------------------|-------------------------|-------------------------|------------------------|-------------------------|-------------------------|-----------------------------|-----------------------|
| $\{w_p(r_p), n_g\}$                                      | ELUCID  | $0.39^{+0.24}_{-0.22}$ | $11.99^{+0.11}_{-0.06}$ | $13.28^{+0.12}_{-0.10}$ | $1.09^{+0.09}_{-0.09}$ | $-0.06^{+0.26}_{-0.22}$ | $0.40^{+0.49}_{-0.46}$  | $0.81^{+0.12}_{-0.13}$      | 14.23/14              |
| $\{w_p(r_p), n_g\}$                                      | Bolshoi | $0.30^{+0.28}_{-0.20}$ | $11.92^{+0.11}_{-0.06}$ | $13.24^{+0.15}_{-0.11}$ | $1.10^{+0.10}_{-0.08}$ | $-0.08^{+0.18}_{-0.26}$ | $-0.25^{+0.71}_{-0.59}$ | $0.85^{+0.12}_{-0.13}$      | 13.75/14              |
| $\{w_p(r_p), p(N_8^g), n_g\}$                            | ELUCID  | $0.54^{+0.15}_{-0.23}$ | $12.08^{+0.07}_{-0.06}$ | $13.19^{+0.07}_{-0.06}$ | $1.04^{+0.07}_{-0.06}$ | $-0.17^{+0.08}_{-0.08}$ | $0.08^{+0.16}_{-0.12}$  | $0.74^{+0.10}_{-0.11}$      | 46.48/34              |
| $\{w_p(r_p), p(N_8^g), n_g\}$                            | Bolshoi | $0.22^{+0.09}_{-0.07}$ | $11.95^{+0.03}_{-0.02}$ | $13.13^{+0.06}_{-0.05}$ | $1.02^{+0.06}_{-0.05}$ | $-0.11^{+0.06}_{-0.06}$ | $-0.29^{+0.11}_{-0.11}$ | $0.78^{+0.10}_{-0.09}$      | 41.13/34              |
| $\{w_p(r_p \tilde{N}_8^{g,i}) _{i=1-5}, n_g\}$           | ELUCID  | $0.20^{+0.05}_{-0.05}$ | $11.95^{+0.03}_{-0.03}$ | $13.15^{+0.06}_{-0.04}$ | $1.01^{+0.04}_{-0.03}$ | $-0.04^{+0.07}_{-0.07}$ | $0.25^{+0.13}_{-0.11}$  | $0.77^{+0.09}_{-0.09}$      | 76.28/94              |
| $\{w_p(r_p \tilde{N}_8^{g,i}) _{i=1-5}, n_g\}$           | Bolshoi | $0.19^{+0.06}_{-0.06}$ | $11.97^{+0.03}_{-0.03}$ | $13.07^{+0.05}_{-0.07}$ | $0.93^{+0.03}_{-0.04}$ | $-0.16^{+0.06}_{-0.06}$ | $0.29^{+0.14}_{-0.12}$  | $0.74^{+0.09}_{-0.11}$      | 152.31/94             |
| $\{w_p(r_p \tilde{N}_8^{g,i}) _{i=1-5}, p(N_8^g), n_g\}$ | ELUCID  | $0.27^{+0.14}_{-0.06}$ | $12.02^{+0.04}_{-0.02}$ | $13.18^{+0.06}_{-0.04}$ | $1.02^{+0.05}_{-0.04}$ | $-0.09^{+0.05}_{-0.06}$ | $0.09^{+0.13}_{-0.08}$  | $0.76^{+0.08}_{-0.10}$      | 125.11/114            |
| $\{w_p(r_p \tilde{N}_8^{g,i}) _{i=1-5}, p(N_8^g), n_g\}$ | Bolshoi | $0.20^{+0.05}_{-0.04}$ | $11.98^{+0.02}_{-0.02}$ | $13.12^{+0.04}_{-0.04}$ | $0.99^{+0.03}_{-0.03}$ | $-0.11^{+0.04}_{-0.05}$ | $-0.02^{+0.09}_{-0.08}$ | $0.77^{+0.07}_{-0.09}$      | 167.22/114            |

that there is still some residual impact of cosmic variance between ELUCID and SDSS that is not included in our uncertainties, our current fiducial constraint indicates no evidence for having a strong halo assembly bias in the local Universe for the population of galaxies selected by  $M_* \geq 10^{10.2} h^{-2} M_\odot$ , typical of galaxies in the SDSS Main Galaxy redshift survey. In Figure 7 we show the comparison between the overdensity-dependent cross-correlation functions predicted by our best-fitting model with ELUCID (coloured curves) and the data (circles with errorbars). The inset panel shows the comparison for the PDF of galaxy overdensity. The best-fitting prediction yields a value of  $\chi^2/\text{d.o.f.}=134.95/114$ , indicating a satisfactory goodness of fit to the data, with each of the observables well described at all scales. This is an impressive testament to the ability of the combination of our HOD model and the ELUCID reconstruction to describe the distribution and clustering of galaxies in the local Universe, without the need to invoke any strong galaxy assembly bias effect. Previous successes of HOD models in reproducing the global  $w_p(r_p)$  and 1-point PDF did not guarantee success in reproducing the observed correlation functions of galaxies in  $N_8^g$  quintiles, which provide a much more detailed characterization of environment-dependent clustering.

## 8 Conclusions

In this paper, we have investigated the level of galaxy assembly bias in the local Universe by performing a comprehensive HOD modelling of the overdensity environment and projected clustering of SDSS galaxies, using the state-of-the-art constrained simulation ELUCID that accurately reconstructed the initial density pertur-

bations of the SDSS volume.

For modelling galaxy assembly bias, we extend the standard HOD prescription by including separate levels of central and satellite assembly bias, parametrized by  $Q_{\text{cen}}$  and  $Q_{\text{sat}}$ , respectively. In particular, we extend the galaxy assembly bias parametrization of Wibking et al. [92] and Salcedo et al. [69] to include satellite assembly bias in the form of the parameter  $Q_{\text{sat}}$  (see also [96]). The parameter  $Q_{\text{sat}}$  allows the satellite occupation to vary at fixed mass based on the large scale environment by varying  $\log M_1$  on a halo-by-halo basis. The parameter  $Q_{\text{cen}}$  (called  $Q_{\text{env}}$  in [92] and [69]) acts similarly by modifying  $\log M_{\min}$ .

We have employed a variety of data vectors consisting of one and two-point galaxy statistics. Extensive mock tests demonstrate that using a non-constrained simulation could potentially show false evidence of galaxy assembly bias for some of the data vectors that are sensitive to the cosmic variance. Among the four data vectors we tested, we identify the combination of correlation functions of galaxy quintiles selected by galaxy number count  $N_8^g$ , the probability density distribution of  $N_8^g$ , and the overall galaxy number density  $n_g$ , as the fiducial input for our analysis with the SDSS data, because of its stringent constraining power.

Applying our extended HOD model on the ELUCID simulation to fit the SDSS galaxies, our fiducial analysis yields stringent constraints of the level of galaxy assembly bias in SDSS, with  $Q_{\text{cen}} = -0.09^{+0.05}_{-0.06}$  and  $Q_{\text{sat}} = 0.09^{+0.13}_{-0.08}$ , respectively. Therefore, we do not find evidence for the existence of a strong ( $> 2\sigma$ ) galaxy assembly bias within the SDSS main galaxy sample, despite examining statistics that would be sensitive to such bias if it were present. The best-fitting model provides an excel-

lent description of the overdensity environment of each *individual* observed galaxy, as well as the projected clustering of galaxies within different overdensity environments, ranging from voids to average field to clusters and super-clusters.

Although the combined one- and two-point statistics measured from SDSS are consistent with having no galaxy assembly bias, our constraint is dominated by the statistical uncertainties, with residual cosmic variance effect due to imperfect ELUCID reconstruction in the underdense regions. With current and upcoming spectroscopic surveys like Dark Energy Spectroscopic Instrument (DESI; [24]) and the Prime Focus Spectrograph (PFS; [80]), the uncertainties of our method will be greatly reduced due to the orders-of-magnitude increase in the observed number of spectra, as well as a thorough removal of the cosmic variance with the ever-increasing survey volume.

*We thank the anonymous referees for helpful suggestions that have greatly improved the manuscript, and Ben Wibking, Hao-Yi Wu, and Zheng Zheng for stimulating discussions about this work. YZ and HYW acknowledge the support by the National Key Basic Research and Development Program of China (No. 2018YFA0404504). YZ acknowledges the support by the National Science Foundation of China (11873038, 11621303, 11890692, 12173024), the science research grants from the China Manned Space Project (No. CMS-CSST-2021-A01, CMS-CSST-2021-A02, CMS-CSST-2021-B01), the National One-Thousand Youth Talent Program of China, and the STJU start-up fund (No. WF220407220). ANS thanks SJTU and TDLI for hospitality. ANS was supported by a Department of Energy Computational Science Graduate Fellowship. This material is based upon work supported by the U.S. Department of Energy, Office of Science, Office of Advanced Scientific Computing Research, Department of Energy Computational Science Graduate Fellowship under Award Number DE-FG02-97ER25308. YZ, XHY, and YPJ acknowledge the support by the “111” project of the Ministry of Education under grant No. B20019. YZ thanks Cathy Huang for her hospitality during his visit to the Zhangjiang Hi-Technology Park where he worked on this project. HYW is supported by the National Science Foundation of China (11733004, 11421303, 11890693). DW acknowledges support of NSF grant AST 2009735. The Bolshoi simulations have been performed within the Bolshoi project of the University of California High-Performance AstroComputing Center (UC-HiPACC) and were run at the NASA Ames Research Center. The CosmoSim database used in this paper is a service by the Leibniz-Institute for Astrophysics Potsdam (AIP). Simulations were analyzed in part on computational resources of the Ohio Supercomputer Center [63], with resources supported in part by the Center for Cosmology and AstroParticle Physics at the Ohio State University. We gratefully acknowledge the use of the MATPLOTLIB software package [40] and the GNU Scientific library [29]. This research has made use of the SAO/NASA Astrophysics Data System. This report was prepared as an account of work sponsored by an agency of the United States Government. Neither the United State Government nor any agency thereof, nor any of their employees, makes any warranty, express or implied, or assumes any legal liability or responsibility for the accuracy, completeness, or usefulness of any information, apparatus, product, or process disclosed, or represents that its use would not in-*

*fringe on privately owned rights. Reference herein to any specific commercial product, process, or service by trade name, trademark, manufacturer or otherwise does not necessarily constitute or imply its endorsement, recommendation, or favoring by the United States Government or any agency thereof. The views and opinions of authors expressed herein do not necessarily state or reflect those of the United State Government or any agency thereof.*

**Conflict of interest** The authors declare that they have no conflict of interest.

- 1 K. N. Abazajian, J. K. Adelman-McCarthy, M. A. Agüeros, S. S. Allam, C. Allende Prieto, D. An, K. S. J. Anderson, S. F. Anderson, J. Annis, N. A. Bahcall, C. A. L. Bailer-Jones, J. C. Barentine, B. A. Bassett, A. C. Becker, T. C. Beers, E. F. Bell, V. Belokurov, A. A. Berlind, E. F. Berman, M. Bernardi, S. J. Bickerton, D. Bizyaev, J. P. Blakeslee, M. R. Blanton, J. J. Bochanski, W. N. Boroski, H. J. Brewington, J. Brinchmann, J. Brinkmann, R. J. Brunner, T. Budavári, L. N. Carey, S. Carliles, M. A. Carr, F. J. Castander, D. Cinabro, A. J. Connolly, I. Csabai, C. E. Cunha, P. C. Czarapata, J. R. A. Davenport, E. de Haas, B. Dilday, M. Doi, D. J. Eisenstein, M. L. Evans, N. W. Evans, X. Fan, S. D. Friedman, J. A. Frieman, M. Fukugita, B. T. Gänsicke, E. Gates, B. Gillespie, G. Gilmore, B. Gonzalez, C. F. Gonzalez, E. K. Grebel, J. E. Gunn, Z. Györy, P. B. Hall, P. Harding, F. H. Harris, M. Harvanek, S. L. Hawley, J. J. E. Hayes, T. M. Heckman, J. S. Hendry, G. S. Hennessy, R. B. Hindsley, J. Hobbitt, C. J. Hogan, D. W. Hogg, J. A. Holtzman, J. B. Hyde, S.-i. Ichikawa, T. Ichikawa, M. Im, Ž. Ivezić, S. Jester, L. Jiang, J. A. Johnson, A. M. Jorgensen, M. Jurić, S. M. Kent, R. Kessler, S. J. Kleinman, G. R. Knapp, K. Konishi, R. G. Kron, J. Krzesinski, N. Kuropatkin, H. Lampeitl, S. Lebedeva, M. G. Lee, Y. S. Lee, R. French Leger, S. Lépine, N. Li, M. Lima, H. Lin, D. C. Long, C. P. Loomis, J. Loveday, R. H. Lupton, E. Magnier, O. Malanushenko, V. Malanushenko, R. Mandelbaum, B. Margon, J. P. Marriner, D. Martínez-Delgado, T. Matsubara, P. M. McGehee, T. A. McKay, A. Meiksin, H. L. Morrison, F. Mullally, J. A. Munn, T. Murphy, T. Nash, A. Nebot, J. Neilsen, Eric H., H. J. Newberg, P. R. Newman, R. C. Nichol, T. Nicinski, M. Nieto-Santisteban, A. Nitta, S. Okamura, D. J. Oravetz, J. P. Ostriker, R. Owen, N. Padmanabhan, K. Pan, C. Park, G. Pauls, J. Peoples, John, W. J. Percival, J. R. Pier, A. C. Pope, D. Pourbaix, P. A. Price, N. Purger, T. Quinn, M. J. Raddick, P. Re Fiorentin, G. T. Richards, M. W. Richmond, A. G. Riess, H.-W. Rix, C. M. Rockosi, M. Sako, D. J. Schlegel, D. P. Schneider, R.-D. Scholz, M. R. Schreiber, A. D. Schwobe, U. Seljak, B. Sesar, E. Sheldon, K. Shimasaku, V. C. Sibley, A. E. Simmons, T. Sivarani, J. Allyn Smith, M. C. Smith, V. Smolčić, S. A. Snedden, A. Stebbins, M. Steinmetz, C. Stoughton, M. A. Strauss, M. SubbaRao, Y. Suto, A. S. Szalay, I. Szapudi, P. Szkody, M. Tanaka, M. Tegmark, L. F. A. Teodoro, A. R. Thakar, C. A. Tremonti, D. L. Tucker, A. Uomoto, D. E. Vanden Berk, J. Vandenberg, S. Vidrih, M. S. Vogeley, W. Voges, N. P. Vogt, Y. Wadadekar, S. Watters, D. H. Weinberg, A. A. West, S. D. M. White, B. C. Wilhite, A. C. Wonders, B. Yanny, D. R. Yocum, D. G. York, I. Zehavi, S. Zibetti, and D. B. Zucker. The Seventh Data Release of the Sloan Digital Sky Survey. *ApJs*, 182(2):543–558, June 2009.
- 2 U. Abbas and R. K. Sheth. Strong clustering of underdense regions and the environmental dependence of clustering from Gaussian initial conditions. *MNRAS*, 378(2):641–

- 648, June 2007.
- 3 S. Alam, Y. Zu, J. A. Peacock, and R. Mandelbaum. Cosmic web dependence of galaxy clustering and quenching in SDSS. *MNRAS*, 483(4):4501–4517, Mar 2019.
  - 4 M. C. Artale, I. Zehavi, S. Contreras, and P. Norberg. The impact of assembly bias on the halo occupation in hydrodynamical simulations. *MNRAS*, 480(3):3978–3992, Nov 2018.
  - 5 J. M. Bardeen, J. R. Bond, N. Kaiser, and A. S. Szalay. The Statistics of Peaks of Gaussian Random Fields. *ApJ*, 304:15, May 1986.
  - 6 P. S. Behroozi, R. H. Wechsler, and H.-Y. Wu. The ROCKSTAR Phase-space Temporal Halo Finder and the Velocity Offsets of Cluster Cores. *ApJ*, 762:109, Jan. 2013.
  - 7 G. D. Beltz-Mohrmann, A. A. Berlind, and A. O. Szezwicw. Testing the accuracy of halo occupation distribution modelling using hydrodynamic simulations. *MNRAS*, 491(4):5771–5788, Feb. 2020.
  - 8 A. A. Berlind and D. H. Weinberg. The Halo Occupation Distribution: Toward an Empirical Determination of the Relation between Galaxies and Mass. *ApJ*, 575:587–616, Aug. 2002.
  - 9 M. R. Blanton, D. J. Schlegel, M. A. Strauss, J. Brinkmann, D. Finkbeiner, M. Fukugita, J. E. Gunn, D. W. Hogg, Ž. Ivezić, G. R. Knapp, R. H. Lupton, J. A. Munn, D. P. Schneider, M. Tegmark, and I. Zehavi. New York University Value-Added Galaxy Catalog: A Galaxy Catalog Based on New Public Surveys. *AJ*, 129(6):2562–2578, June 2005.
  - 10 J. R. Bond, S. Cole, G. Efstathiou, and N. Kaiser. Excursion Set Mass Functions for Hierarchical Gaussian Fluctuations. *ApJ*, 379:440, Oct. 1991.
  - 11 S. Bose, D. J. Eisenstein, L. Hernquist, A. Pillepich, D. Nelson, F. Marinacci, V. Springel, and M. Vogelsberger. Revealing the galaxy-halo connection in IllustrisTNG. *MNRAS*, 490(4):5693–5711, Dec. 2019.
  - 12 R. G. Bower. The evolution of groups of galaxies in the Press-Schechter formalism. *MNRAS*, 248:332–352, Jan. 1991.
  - 13 G. Bruzual and S. Charlot. Stellar population synthesis at the resolution of 2003. *MNRAS*, 344(4):1000–1028, Oct. 2003.
  - 14 V. F. Calderon, A. A. Berlind, and M. Sinha. Small- and large-scale galactic conformity in SDSS DR7. *MNRAS*, 480(2):2031–2045, Oct. 2018.
  - 15 G. Chabrier. Galactic Stellar and Substellar Initial Mass Function. *PASP*, 115(809):763–795, July 2003.
  - 16 J. Chaves-Montero, R. E. Angulo, J. Schaye, M. Schaller, R. A. Crain, M. Furlong, and T. Theuns. Subhalo abundance matching and assembly bias in the EAGLE simulation. *MNRAS*, 460(3):3100–3118, Aug. 2016.
  - 17 Y. Chen, H. J. Mo, C. Li, H. Wang, X. Yang, S. Zhou, and Y. Zhang. ELUCID. VI. Cosmic Variance of the Galaxy Distribution in the Local Universe. *ApJ*, 872(2):180, Feb. 2019.
  - 18 S. Contreras, R. E. Angulo, and M. Zennaro. A flexible modelling of galaxy assembly bias. *MNRAS*, 504(4):5205–5220, July 2021.
  - 19 S. Contreras, I. Zehavi, N. Padilla, C. M. Baugh, E. Jiménez, and I. Lacerna. The evolution of assembly bias. *MNRAS*, 484(1):1133–1148, Mar 2019.
  - 20 A. Cooray. Halo model at its best: constraints on conditional luminosity functions from measured galaxy statistics. *MNRAS*, 365(3):842–866, Jan. 2006.
  - 21 A. Cooray and R. Sheth. Halo models of large scale structure. *Phys. Rep.*, 372(1):1–129, Dec. 2002.
  - 22 D. J. Croton, L. Gao, and S. D. M. White. Halo assembly bias and its effects on galaxy clustering. *MNRAS*, 374(4):1303–1309, Feb. 2007.
  - 23 K. S. Dawson, D. J. Schlegel, C. P. Ahn, S. F. Anderson, É. Aubourg, S. Bailey, R. H. Barkhouser, J. E. Bautista, A. Beifiori, A. A. Berlind, V. Bhardwaj, D. Bizyaev, C. H. Blake, M. R. Blanton, M. Blomqvist, A. S. Bolton, A. Borde, J. Bovy, W. N. Brandt, H. Brewington, J. Brinkmann, P. J. Brown, J. R. Brownstein, K. Bundy, N. G. Busca, W. Carithers, A. R. Carnero, M. A. Carr, Y. Chen, J. Comparat, N. Connolly, F. Cope, R. A. C. Croft, A. J. Cuesta, L. N. da Costa, J. R. A. Davenport, T. Delubac, R. de Putter, S. Dhital, A. Ealet, G. L. Ebelke, D. J. Eisenstein, S. Escoffier, X. Fan, N. Filiz Ak, H. Finley, A. Font-Ribera, R. Génova-Santos, J. E. Gunn, H. Guo, D. Haggard, P. B. Hall, J.-C. Hamilton, B. Harris, D. W. Harris, S. Ho, D. W. Hogg, D. Holder, K. Honscheid, J. Huehnerhoff, B. Jordan, W. P. Jordan, G. Kauffmann, E. A. Kazin, D. Kirkby, M. A. Klaene, J.-P. Kneib, J.-M. Le Goff, K.-G. Lee, D. C. Long, C. P. Loomis, B. Lundgren, R. H. Lupton, M. A. G. Maia, M. Makler, E. Malanushenko, V. Malanushenko, R. Mandelbaum, M. Manera, C. Maraston, D. Margala, K. L. Masters, C. K. McBride, P. McDonald, I. D. McGreer, R. G. McMahon, O. Mena, J. Miralda-Escudé, A. D. Montero-Dorta, F. Montesano, D. Muna, A. D. Myers, T. Naugle, R. C. Nichol, P. Noterdaeme, S. E. Nuza, M. D. Olmstead, A. Oravetz, D. J. Oravetz, R. Owen, N. Padmanabhan, N. Palanque-Delabrouille, K. Pan, J. K. Parejko, I. Pâris, W. J. Percival, I. Pérez-Fournon, I. Pérez-Ráfol, P. Petitjean, R. Pfaffenberger, J. Pforr, M. M. Pieri, F. Prada, A. M. Price-Whelan, M. J. Raddick, R. Rebolo, J. Rich, G. T. Richards, C. M. Rockosi, N. A. Roe, A. J. Ross, N. P. Ross, G. Rossi, J. A. Rubiño-Martín, L. Samushia, A. G. Sánchez, C. Sayres, S. J. Schmidt, D. P. Schneider, C. G. Scóccola, H.-J. Seo, A. Shelden, E. Shelden, Y. Shen, Y. Shu, A. Slosar, S. A. Smee, S. A. Snedden, F. Stauffer, O. Steele, M. A. Strauss, A. Streblyanska, N. Suzuki, M. E. C. Swanson, T. Tal, M. Tanaka, D. Thomas, J. L. Tinker, R. Tojeiro, C. A. Tremonti, M. Vargas Magaña, L. Verde, M. Viel, D. A. Wake, M. Watson, B. A. Weaver, D. H. Weinberg, B. J. Weiner, A. A. West, M. White, W. M. Wood-Vasey, C. Yeche, I. Zehavi, G.-B. Zhao, and Z. Zheng. The Baryon Oscillation Spectroscopic Survey of SDSS-III. *AJ*, 145:10, Jan. 2013.
  - 24 DESI Collaboration, A. Aghamousa, J. Aguilar, S. Ahlen, S. Alam, L. E. Allen, C. Allende Prieto, J. Annis, S. Bailey, C. Balland, O. Ballester, C. Baltay, L. Beaufore, C. Bebek, T. C. Beers, E. F. Bell, J. L. Bernal, R. Besuner, F. Beutler, C. Blake, H. Bleuler, M. Blomqvist, R. Blum, A. S. Bolton, C. Briceno, D. Brooks, J. R. Brownstein, E. Buckley-Geer, A. Burden, E. Burtin, N. G. Busca, R. N. Cahn, Y.-C. Cai, L. Cardiel-Sas, R. G. Carlberg, P.-H. Carton, R. Casas, F. J. Castander, J. L. Cervantes-Cota, T. M. Claybaugh, M. Close, C. T. Coker, S. Cole, J. Comparat, A. P. Cooper, M. C. Cousinou, M. Coce, J.-G. Cuby, D. P. Cunningham, T. M. Davis, K. S. Dawson, A. de la Macorra, J. De Vicente, T. Delubac, M. Derwent, A. Dey, G. Dhungana, Z. Ding, P. Doel, Y. T. Duan, A. Ealet, J. Edelman, S. Eftekharzadeh, D. J. Eisenstein, A. Elliott, S. Escoffier, M. Evatt, P. Fagrelus, X. Fan, K. Fanning, A. Farahi, J. Farihi, G. Favole, Y. Feng, E. Fernandez, J. R. Findlay, D. P. Finkbeiner, M. J. Fitzpatrick, B. Flaugher, S. Flender, A. Font-Ribera, J. E. Forero-Romero, P. Fosalba, C. S. Frenk, M. Fumagalli, B. T. Gaensicke, G. Gallo, J. Garcia-Bellido, E. Gaztanaga, N. Pietro

- Gentile Fusillo, T. Gerard, I. Gershkovich, T. Giannantonio, D. Gillet, G. Gonzalez-de-Rivera, V. Gonzalez-Perez, S. Gott, O. Graur, G. Gutierrez, J. Guy, S. Habib, H. Heetderks, I. Heetderks, K. Heitmann, W. A. Hellwing, D. A. Herrera, S. Ho, S. Holland, K. Honscheid, E. Huff, T. A. Hutchinson, D. Huterer, H. S. Hwang, J. M. Illa Laguna, Y. Ishikawa, D. Jacobs, N. Jeffrey, P. Jelinsky, E. Jennings, L. Jiang, J. Jimenez, J. Johnson, R. Joyce, E. Jullo, S. Juneau, S. Kama, A. Karcher, S. Karkar, R. Kehoe, N. Kennamer, S. Kent, M. Kilbinger, A. G. Kim, D. Kirkby, T. Kisner, E. Kitanidis, J.-P. Kneib, S. Koposov, E. Kovacs, K. Koyama, A. Kremin, R. Kron, L. Kronig, A. Kueter-Young, C. G. Lacey, R. Lafever, O. Lahav, A. Lambert, M. Lampton, M. Land riau, D. Lang, T. R. Lauer, J.-M. Le Goff, L. Le Guillou, A. Le Van Suu, J. H. Lee, S.-J. Lee, D. Leitner, M. Lesser, M. E. Levi, B. L'Huillier, B. Li, M. Liang, H. Lin, E. Linder, S. R. Loebman, Z. Lukić, J. Ma, N. MacCrann, C. Magneville, L. Makarem, M. Manera, C. J. Manser, R. Marshall, P. Martini, R. Massey, T. Matheson, J. McCauley, P. McDonald, I. D. McGreer, A. Meisner, N. Metcalfe, T. N. Miller, R. Miquel, J. Moustakas, A. Myers, M. Naik, J. A. Newman, R. C. Nichol, A. Nicola, L. Nicolati da Costa, J. Nie, G. Niz, P. Norberg, B. Nord, D. Norman, P. Nugent, T. O'Brien, M. Oh, K. A. G. Olsen, C. Padilla, H. Padmanabhan, N. Padmanabhan, N. Palanque-Delabrouille, A. Palmese, D. Papalardo, I. Pâris, C. Park, A. Patej, J. A. Peacock, H. V. Peiris, X. Peng, W. J. Percival, S. Perruchot, M. M. Pieri, R. Pogge, J. E. Pollack, C. Poppett, F. Prada, A. Prakash, R. G. Probst, D. Rabinowitz, A. Raichoor, C. H. Ree, A. Refregier, X. Regal, B. Reid, K. Reil, M. Rezaie, C. M. Rockosi, N. Roe, S. Ronayette, A. Roodman, A. J. Ross, N. P. Ross, G. Rossi, E. Rozo, V. Ruhlmann-Kleider, E. S. Rykoff, C. Sabiu, L. Samushia, E. Sanchez, J. Sanchez, D. J. Schlegel, M. Schneider, M. Schubnell, A. Secroun, U. Seljak, H.-J. Seo, S. Serrano, A. Shafieloo, H. Shan, R. Sharples, M. J. Sholl, W. V. Shourt, J. H. Silber, D. R. Silva, M. M. Sirk, A. Slosar, A. Smith, G. F. Smoot, D. Som, Y.-S. Song, D. Sprayberry, R. Staten, A. Stefanik, G. Tarle, S. Sien Tie, J. L. Tinker, R. Tojeiro, F. Valdes, O. Valenzuela, M. Valuri, M. Vargas-Magana, L. Verde, A. R. Walker, J. Wang, Y. Wang, B. A. Weaver, C. Weaverdyck, R. H. Wechsler, D. H. Weinberg, M. White, Q. Yang, C. Yeche, T. Zhang, G.-B. Zhao, Y. Zheng, X. Zhou, Z. Zhou, Y. Zhu, H. Zou, and Y. Zu. The DESI Experiment Part I: Science, Targeting, and Survey Design. *arXiv e-prints*, page arXiv:1611.00036, Oct. 2016.
- 25 J. Dunkley, E. Komatsu, M. R.olta, D. N. Spergel, D. Larson, G. Hinshaw, L. Page, C. L. Bennett, B. Gold, and N. Jarosik. Five-Year Wilkinson Microwave Anisotropy Probe Observations: Likelihoods and Parameters from the WMAP Data. *ApJs*, 180(2):306–329, Feb 2009.
- 26 A. Faltenbacher, A. Finoguenov, and N. Drory. The Halo Mass Function Conditioned on Density from the Millennium Simulation: Insights into Missing Baryons and Galaxy Mass Functions. *ApJ*, 712(1):484–493, Mar. 2010.
- 27 A. Faltenbacher and S. D. M. White. Assembly Bias and the Dynamical Structure of Dark Matter Halos. *ApJ*, 708:469–473, Jan. 2010.
- 28 D. Foreman-Mackey, D. W. Hogg, D. Lang, and J. Goodman. emcee: The MCMC Hammer. *PASP*, 125(925):306, Mar 2013.
- 29 M. Galassi, J. Davies, J. Theiler, B. Gough, G. Jungman, P. Alken, M. Booth, and F. Rossi. *GNU Scientific Library Reference Manual*, 3 edition, Jan. 2009.
- 30 L. Gao, V. Springel, and S. D. M. White. The age dependence of halo clustering. *MNRAS*, 363:L66–L70, Oct. 2005.
- 31 L. Gao and S. D. M. White. Assembly bias in the clustering of dark matter haloes. *MNRAS*, 377:L5–L9, Apr. 2007.
- 32 J. Goodman and J. Weare. Ensemble samplers with affine invariance. *Communications in Applied Mathematics and Computational Science*, 5(1):65–80, Jan 2010.
- 33 I. Gott, J. Richard, M. Jurić, D. Schlegel, F. Hoyle, M. Vogele, M. Tegmark, N. Bahcall, and J. Brinkmann. A Map of the Universe. *ApJ*, 624(2):463–484, May 2005.
- 34 H. Guo, Z. Zheng, I. Zehavi, P. S. Behroozi, C.-H. Chuang, J. Comparat, G. Favole, S. Gottloeber, A. Klypin, F. Prada, D. H. Weinberg, and G. Yepes. Redshift-space clustering of SDSS galaxies - luminosity dependence, halo occupation distribution, and velocity bias. *MNRAS*, 453:4368–4383, Nov. 2015.
- 35 B. Hadzhiyska, S. Liu, R. S. Somerville, A. Gabrielpillai, S. Bose, D. Eisenstein, and L. Hernquist. Galaxy assembly bias and large-scale distribution: a comparison between IllustrisTNG and a semi-analytic model. *MNRAS*, 508(1):698–718, Nov. 2021.
- 36 G. Harker, S. Cole, J. Helly, C. Frenk, and A. Jenkins. A marked correlation function analysis of halo formation times in the Millennium Simulation. *MNRAS*, 367:1039–1049, Apr. 2006.
- 37 A. P. Hearin and D. F. Watson. The dark side of galaxy colour. *MNRAS*, 435(2):1313–1324, Oct. 2013.
- 38 A. P. Hearin, D. F. Watson, and F. C. van den Bosch. Beyond halo mass: galactic conformity as a smoking gun of central galaxy assembly bias. *MNRAS*, 452(2):1958–1969, Sept. 2015.
- 39 A. P. Hearin, A. R. Zentner, F. C. van den Bosch, D. Campbell, and E. Tollerud. Introducing decorated HODs: modelling assembly bias in the galaxy-halo connection. *MNRAS*, 460:2552–2570, Aug. 2016.
- 40 J. D. Hunter. Matplotlib: A 2d graphics environment. *Computing In Science & Engineering*, 9(3):90–95, 2007.
- 41 Y. P. Jing, H. J. Mo, and G. Börner. Spatial Correlation Function and Pairwise Velocity Dispersion of Galaxies: Cold Dark Matter Models versus the Las Campanas Survey. *ApJ*, 494:1–12, Feb. 1998.
- 42 Y. P. Jing, Y. Suto, and H. J. Mo. The Dependence of Dark Halo Clustering on Formation Epoch and Concentration Parameter. *ApJ*, 657(2):664–668, March 2007.
- 43 J. W. Johnson, A. H. Maller, A. A. Berlind, M. Sinha, and J. K. Holley-Bockelmann. The secondary spin bias of dark matter haloes. *MNRAS*, 486(1):1156–1166, June 2019.
- 44 N. Kaiser. Evolution and clustering of rich clusters. *MNRAS*, 222:323–345, Sep 1986.
- 45 G. Kauffmann, T. M. Heckman, S. D. M. White, S. Charlot, C. Tremonti, J. Brinchmann, G. Bruzual, E. W. Peng, M. Seibert, M. Bernardi, M. Blanton, J. Brinkmann, F. Castander, I. Csábai, M. Fukugita, Z. Ivezic, J. A. Munn, R. C. Nichol, N. Padmanabhan, A. R. Thakar, D. H. Weinberg, and D. York. Stellar masses and star formation histories for  $10^5$  galaxies from the Sloan Digital Sky Survey. *MNRAS*, 341(1):33–53, May 2003.
- 46 G. Kauffmann, C. Li, W. Zhang, and S. Weinmann. A re-examination of galactic conformity and a comparison with semi-analytic models of galaxy formation. *MNRAS*, 430(2):1447–1456, Apr. 2013.
- 47 A. A. Klypin, S. Trujillo-Gomez, and J. Primack. Dark Matter Halos in the Standard Cosmological Model: Results from the Bolshoi Simulation. *ApJ*, 740(2):102, Oct. 2011.

- 48 E. Komatsu, K. M. Smith, J. Dunkley, C. L. Bennett, B. Gold, G. Hinshaw, N. Jarosik, D. Larson, M. R.olta, L. Page, D. N. Spergel, M. Halpern, R. S. Hill, A. Kogut, M. Limon, S. S. Meyer, N. Odegard, G. S. Tucker, J. L. Weiland, E. Wollack, and E. L. Wright. Seven-year Wilkinson Microwave Anisotropy Probe (WMAP) Observations: Cosmological Interpretation. *ApJs*, 192:18, Feb. 2011.
- 49 A. V. Kravtsov, A. A. Berlind, R. H. Wechsler, A. A. Klypin, S. Gottlöber, B. Allgood, and J. R. Primack. The Dark Side of the Halo Occupation Distribution. *ApJ*, 609:35–49, July 2004.
- 50 A. Leauthaud, J. Tinker, K. Bundy, P. S. Behroozi, R. Massey, J. Rhodes, M. R. George, J.-P. Kneib, A. Benson, R. H. Wechsler, M. T. Busha, P. Capak, M. Cortés, O. Ilbert, A. M. Koekemoer, O. Le Fèvre, S. Lilly, H. J. McCracken, M. Salvato, T. Schrabback, N. Scoville, T. Smith, and J. E. Taylor. New Constraints on the Evolution of the Stellar-to-dark Matter Connection: A Combined Analysis of Galaxy-Galaxy Lensing, Clustering, and Stellar Mass Functions from  $z = 0.2$  to  $z = 1$ . *ApJ*, 744(2):159, Jan. 2012.
- 51 G. Lemson and G. Kauffmann. Environmental influences on dark matter haloes and consequences for the galaxies within them. *MNRAS*, 302(1):111–117, Jan. 1999.
- 52 Y. Li, H. J. Mo, and L. Gao. On halo formation times and assembly bias. *MNRAS*, 389:1419–1426, Sept. 2008.
- 53 Y.-T. Lin, R. Mandelbaum, Y.-H. Huang, H.-J. Huang, N. Dalal, B. Diemer, H.-Y. Jian, and A. Kravtsov. On Detecting Halo Assembly Bias with Galaxy Populations. *ApJ*, 819(2):119, Mar. 2016.
- 54 C.-P. Ma and J. N. Fry. Deriving the Nonlinear Cosmological Power Spectrum and Bispectrum from Analytic Dark Matter Halo Profiles and Mass Functions. *ApJ*, 543(2):503–513, Nov. 2000.
- 55 R. Mandelbaum, U. Seljak, G. Kauffmann, C. M. Hirata, and J. Brinkmann. Galaxy halo masses and satellite fractions from galaxy-galaxy lensing in the Sloan Digital Sky Survey: stellar mass, luminosity, morphology and environment dependencies. *MNRAS*, 368(2):715–731, May 2006.
- 56 Y.-Y. Mao, A. R. Zentner, and R. H. Wechsler. Beyond assembly bias: exploring secondary halo biases for cluster-size haloes. *MNRAS*, 474:5143–5157, Mar. 2018.
- 57 K. S. McCarthy, Z. Zheng, and H. Guo. The effects of galaxy assembly bias on the inference of growth rate from redshift-space distortions. *MNRAS*, 487(2):2424–2440, Aug. 2019.
- 58 J. E. McEwen and D. H. Weinberg. The effects of assembly bias on the inference of matter clustering from galaxy-galaxy lensing and galaxy clustering. *MNRAS*, 477:4348–4361, July 2018.
- 59 H. J. Mo and S. D. M. White. An analytic model for the spatial clustering of dark matter haloes. *MNRAS*, 282(2):347–361, Sept. 1996.
- 60 A. D. Montero-Dorta, E. Pérez, F. Prada, S. Rodríguez-Torres, G. Favole, A. Klypin, R. Cid Fernandes, R. M. González Delgado, A. Domínguez, A. S. Bolton, R. García-Benito, E. Jullo, and A. Niemic. The Dependence of Galaxy Clustering on Stellar-mass Assembly History for LRGs. *ApJL*, 848(1):L2, Oct. 2017.
- 61 J. F. Navarro, C. S. Frenk, and S. D. M. White. A Universal Density Profile from Hierarchical Clustering. *ApJ*, 490:493–508, Dec. 1997.
- 62 A. Niemic, E. Jullo, A. D. Montero-Dorta, F. Prada, S. Rodríguez-Torres, E. Perez, A. Klypin, T. Erben, M. Makler, B. Moraes, M. E. S. Pereira, and H. Shan. Probing galaxy assembly bias with LRG weak lensing observations. *MNRAS*, 477:L1–L5, June 2018.
- 63 Ohio Supercomputer Center. Ohio supercomputer center. <http://osc.edu/ark:/19495/f5s1ph73>, 1987.
- 64 A. Paranjape, O. Hahn, and R. K. Sheth. Halo assembly bias and the tidal anisotropy of the local halo environment. *MNRAS*, 476(3):3631–3647, May 2018.
- 65 J. A. Peacock and R. E. Smith. Halo occupation numbers and galaxy bias. *MNRAS*, 318(4):1144–1156, Nov 2000.
- 66 Planck Collaboration, P. A. R. Ade, N. Aghanim, M. Arnaud, M. Ashdown, J. Aumont, C. Baccigalupi, A. J. Banday, R. B. Barreiro, J. G. Bartlett, and et al. Planck 2015 results. XIII. Cosmological parameters. *A&A*, 594:A13, Sept. 2016.
- 67 W. H. Press and P. Schechter. Formation of Galaxies and Clusters of Galaxies by Self-Similar Gravitational Condensation. *ApJ*, 187:425–438, Feb 1974.
- 68 A. N. Salcedo, A. H. Maller, A. A. Berlind, M. Sinha, C. K. McBride, P. S. Behroozi, R. H. Wechsler, and D. H. Weinberg. Spatial clustering of dark matter haloes: secondary bias, neighbour bias, and the influence of massive neighbours on halo properties. *MNRAS*, 475:4411–4423, Apr. 2018.
- 69 A. N. Salcedo, B. D. Wibking, D. H. Weinberg, H.-Y. Wu, D. Ferrer, D. Eisenstein, and P. Pinto. Cosmology with stacked cluster weak lensing and cluster-galaxy cross-correlations. *MNRAS*, 491(3):3061–3081, Jan 2020.
- 70 S. Salim, R. M. Rich, S. Charlot, J. Brinchmann, B. D. Johnson, D. Schiminovich, M. Seibert, R. Mallery, T. M. Heckman, K. Forster, P. G. Friedman, D. C. Martin, P. Morrissey, S. G. Neff, T. Small, T. K. Wyder, L. Bianchi, J. Donas, Y.-W. Lee, B. F. Madore, B. Milliard, A. S. Szalay, B. Y. Welsh, and S. K. Yi. UV Star Formation Rates in the Local Universe. *ApJs*, 173(2):267–292, Dec. 2007.
- 71 G. Sato-Polito, A. D. Montero-Dorta, L. R. Abramo, F. Prada, and A. Klypin. The dependence of halo bias on age, concentration, and spin. *MNRAS*, 487(2):1570–1579, Aug. 2019.
- 72 R. Scoccimarro, R. K. Sheth, L. Hui, and B. Jain. How Many Galaxies Fit in a Halo? Constraints on Galaxy Formation Efficiency from Spatial Clustering. *ApJ*, 546:20–34, Jan. 2001.
- 73 U. Seljak. Analytic model for galaxy and dark matter clustering. *MNRAS*, 318(1):203–213, Oct 2000.
- 74 R. K. Sheth, H. J. Mo, and G. Tormen. Ellipsoidal collapse and an improved model for the number and spatial distribution of dark matter haloes. *MNRAS*, 323(1):1–12, May 2001.
- 75 R. K. Sheth and G. Tormen. On the environmental dependence of halo formation. *MNRAS*, 350:1385–1390, June 2004.
- 76 L. P. T. Sin, S. J. Lilly, and B. M. B. Henriques. On The Evidence For Large-Scale Galactic Conformity In The Local Universe. *MNRAS*, 471(1):1192–1207, Oct. 2017.
- 77 M. Sinha and L. Garrison. Corrfunc: Blazing fast correlation functions on the CPU. Astrophysics Source Code Library, Mar. 2017.
- 78 V. Springel. The cosmological simulation code GADGET-2. *MNRAS*, 364(4):1105–1134, Dec. 2005.
- 79 M. A. Strauss, D. H. Weinberg, R. H. Lupton, V. K. Narayanan, J. Annis, M. Bernardi, M. Blanton, S. Burles, A. J. Connolly, J. Dalcanton, M. Doi, D. Eisenstein, J. A. Frieman, M. Fukugita, J. E. Gunn, Ž. Ivezić, S. Kent, R. S. J. Kim, G. R. Knapp, R. G. Kron, J. A. Munn, H. J. Newberg, R. C. Nichol, S. Okamura, T. R. Quinn, M. W. Richmond, D. J. Schlegel, K. Shimasaku, M. SubbaRao, A. S. Szalay, D. Vanden Berk, M. S. Vogeley, B. Yanny,

- N. Yasuda, D. G. York, and I. Zehavi. Spectroscopic Target Selection in the Sloan Digital Sky Survey: The Main Galaxy Sample. *AJ*, 124(3):1810–1824, Sept. 2002.
- 80 M. Takada, R. S. Ellis, M. Chiba, J. E. Greene, H. Aihara, N. Arimoto, K. Bundy, J. Cohen, O. Doré, G. Graves, J. E. Gunn, T. Heckman, C. M. Hirata, P. Ho, J.-P. Kneib, O. Le Fèvre, L. Lin, S. More, H. Murayama, T. Nagao, M. Ouchi, M. Seiffert, J. D. Silverman, L. Sodré, D. N. Spergel, M. A. Strauss, H. Sugai, Y. Suto, H. Takami, and R. Wyse. Extragalactic science, cosmology, and Galactic archaeology with the Subaru Prime Focus Spectrograph. *PASJ*, 66(1):R1, Feb. 2014.
- 81 J. L. Tinker, C. Hahn, Y.-Y. Mao, A. R. Wetzel, and C. Conroy. Halo histories versus galaxy properties at  $z = 0$  II: large-scale galactic conformity. *MNRAS*, 477(1):935–945, June 2018.
- 82 F. C. van den Bosch, X. Yang, and H. J. Mo. Linking early- and late-type galaxies to their dark matter haloes. *MNRAS*, 340(3):771–792, Apr. 2003.
- 83 H. Wang, H. J. Mo, Y. P. Jing, Y. Guo, F. C. van den Bosch, and X. Yang. Reconstructing the cosmic density field with the distribution of dark matter haloes. *MNRAS*, 394(1):398–414, Mar. 2009.
- 84 H. Wang, H. J. Mo, X. Yang, Y. P. Jing, and W. P. Lin. ELUCID—Exploring the Local Universe with the Reconstructed Initial Density Field. I. Hamiltonian Markov Chain Monte Carlo Method with Particle Mesh Dynamics. *ApJ*, 794(1):94, Oct. 2014.
- 85 H. Wang, H. J. Mo, X. Yang, Y. Zhang, J. Shi, Y. P. Jing, C. Liu, S. Li, X. Kang, and Y. Gao. ELUCID - Exploring the Local Universe with ReConstructed Initial Density Field III: Constrained Simulation in the SDSS Volume. *ApJ*, 831(2):164, Nov 2016.
- 86 H. Y. Wang, H. J. Mo, and Y. P. Jing. Environmental dependence of cold dark matter halo formation. *MNRAS*, 375:633–639, Feb. 2007.
- 87 K. Wang, Y.-Y. Mao, A. R. Zentner, F. C. van den Bosch, J. U. Lange, C. M. Schafer, A. S. Villarreal, A. P. Hearin, and D. Campbell. How to optimally constrain galaxy assembly bias: supplement projected correlation functions with count-in-cells statistics. *MNRAS*, 488(3):3541–3567, Sep 2019.
- 88 L. Wang, S. M. Weinmann, G. De Lucia, and X. Yang. Detection of galaxy assembly bias. *MNRAS*, 433(1):515–520, July 2013.
- 89 R. H. Wechsler and J. L. Tinker. The Connection Between Galaxies and Their Dark Matter Halos. *ARA&A*, 56:435–487, Sept. 2018.
- 90 R. H. Wechsler, A. R. Zentner, J. S. Bullock, A. V. Kravtsov, and B. Allgood. The Dependence of Halo Clustering on Halo Formation History, Concentration, and Occupation. *ApJ*, 652:71–84, Nov. 2006.
- 91 S. M. Weinmann, F. C. van den Bosch, X. Yang, and H. J. Mo. Properties of galaxy groups in the Sloan Digital Sky Survey - I. The dependence of colour, star formation and morphology on halo mass. *MNRAS*, 366(1):2–28, Feb. 2006.
- 92 B. D. Wibking, A. N. Salcedo, D. H. Weinberg, L. H. Garrison, D. Ferrer, J. Tinker, D. Eisenstein, M. Metchnik, and P. Pinto. Emulating galaxy clustering and galaxy-galaxy lensing into the deeply non-linear regime: methodology, information, and forecasts. *MNRAS*, 484(1):989–1006, Mar 2019.
- 93 H. Xu, Z. Zheng, H. Guo, J. Zhu, and I. Zehavi. On the clustering of faint red galaxies. *MNRAS*, 460(4):3647–3659, Aug. 2016.
- 94 X. Xu, I. Zehavi, and S. Contreras. Dissecting and modelling galaxy assembly bias. *MNRAS*, 502(3):3242–3263, Apr. 2021.
- 95 X. Xu and Z. Zheng. Dependence of halo bias and kinematics on assembly variables. *MNRAS*, 479:1579–1594, Sept. 2018.
- 96 X. Xu and Z. Zheng. Galaxy assembly bias of central galaxies in the Illustris simulation. *MNRAS*, 492(2):2739–2754, Feb. 2020.
- 97 X. Yang, H. J. Mo, and F. C. van den Bosch. Constraining galaxy formation and cosmology with the conditional luminosity function of galaxies. *MNRAS*, 339(4):1057–1080, Mar. 2003.
- 98 X. Yang, H. J. Mo, and F. C. van den Bosch. Observational Evidence for an Age Dependence of Halo Bias. *ApJ*, 638(2):L55–L58, Feb. 2006.
- 99 X. Yang, H. J. Mo, F. C. van den Bosch, and Y. P. Jing. A halo-based galaxy group finder: calibration and application to the 2dFGRS. *MNRAS*, 356(4):1293–1307, Feb. 2005.
- 100 X. Yang, H. J. Mo, F. C. van den Bosch, A. Pasquali, C. Li, and M. Barden. Galaxy Groups in the SDSS DR4. I. The Catalog and Basic Properties. *ApJ*, 671(1):153–170, Dec. 2007.
- 101 X. Yang, Y. Zhang, T. Lu, H. Wang, F. Shi, D. Tweed, S. Li, W. Luo, Y. Lu, and L. Yang. Revealing the Cosmic Web-dependent Halo Bias. *ApJ*, 848(1):60, Oct. 2017.
- 102 S. Yuan, D. J. Eisenstein, and L. H. Garrison. Exploring the squeezed three-point galaxy correlation function with generalized halo occupation distribution models. *MNRAS*, 478(2):2019–2033, Aug. 2018.
- 103 I. Zehavi, S. Contreras, N. Padilla, N. J. Smith, C. M. Baugh, and P. Norberg. The Impact of Assembly Bias on the Galaxy Content of Dark Matter Halos. *ApJ*, 853:84, Jan. 2018.
- 104 I. Zehavi, Z. Zheng, D. H. Weinberg, M. R. Blanton, N. A. Bahcall, A. A. Berlind, J. Brinkmann, J. A. Frieman, J. E. Gunn, R. H. Lupton, R. C. Nichol, W. J. Percival, D. P. Schneider, R. A. Skibba, M. A. Strauss, M. Tegmark, and D. G. York. Galaxy Clustering in the Completed SDSS Redshift Survey: The Dependence on Color and Luminosity. *ApJ*, 736:59, July 2011.
- 105 I. Zehavi, Z. Zheng, D. H. Weinberg, J. A. Frieman, A. A. Berlind, M. R. Blanton, R. Scoccimarro, R. K. Sheth, M. A. Strauss, I. Kayo, Y. Suto, M. Fukugita, O. Nakamura, N. A. Bahcall, J. Brinkmann, J. E. Gunn, G. S. Hennessy, Ž. Ivezić, G. R. Knapp, J. Loveday, A. Meiksin, D. J. Schlegel, D. P. Schneider, I. Szapudi, M. Tegmark, M. S. Vogeley, D. G. York, and SDSS Collaboration. The Luminosity and Color Dependence of the Galaxy Correlation Function. *ApJ*, 630(1):1–27, Sept. 2005.
- 106 A. R. Zentner, A. Hearin, F. C. van den Bosch, J. U. Lange, and A. Villarreal. Constraints on assembly bias from galaxy clustering. *MNRAS*, 485(1):1196–1209, May 2019.
- 107 J. Zhang, C.-P. Ma, and A. Riotto. Dark-matter Halo Assembly Bias: Environmental Dependence in the Non-Markovian Excursion-set Theory. *ApJ*, 782(1):44, Feb. 2014.
- 108 Z. Zheng, A. A. Berlind, D. H. Weinberg, A. J. Benson, C. M. Baugh, S. Cole, R. Davé, C. S. Frenk, N. Katz, and C. G. Lacey. Theoretical Models of the Halo Occupation Distribution: Separating Central and Satellite Galaxies. *ApJ*, 633:791–809, Nov. 2005.
- 109 Y. Zu and R. Mandelbaum. Mapping stellar content to dark matter haloes using galaxy clustering and galaxy-galaxy lensing in the SDSS DR7. *MNRAS*, 454(2):1161–1191, Dec.

- 2015.
- 110 Y. Zu and R. Mandelbaum. Mapping stellar content to dark matter haloes - II. Halo mass is the main driver of galaxy quenching. *MNRAS*, 457(4):4360–4383, Apr. 2016.
- 111 Y. Zu and R. Mandelbaum. Mapping stellar content to dark matter haloes - III. Environmental dependence and conformity of galaxy colours. *MNRAS*, 476(2):1637–1653, May 2018.
- 112 Y. Zu, D. H. Weinberg, E. Rozo, E. S. Sheldon, J. L. Tinker, and M. R. Becker. Cosmological constraints from the large-scale weak lensing of SDSS MaxBCG clusters. *MNRAS*, 439:1628–1647, Apr. 2014.
- 113 Y. Zu, Z. Zheng, G. Zhu, and Y. P. Jing. Environmental Effects on Real-Space and Redshift-Space Galaxy Clustering. *ApJ*, 686(1):41–52, Oct. 2008.

## Appendix A Covariance Matrices

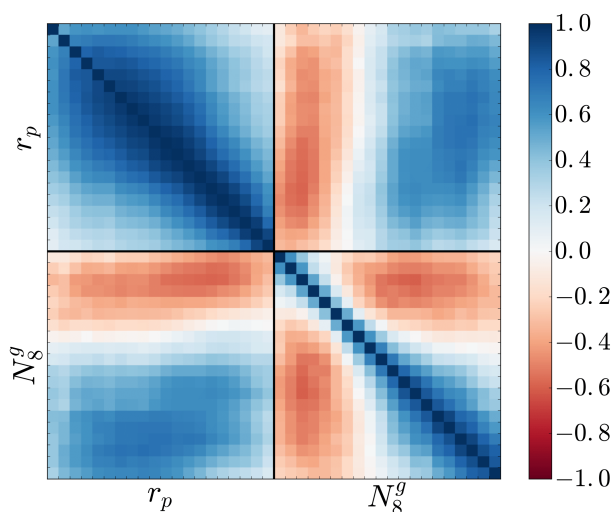


**Figure A1** Correlation matrix of  $\{w_p, p(N_8^g)\}$  calculated directly from SDSS data via jackknife re-sampling, with the correlation coefficients colour-coded by the colour bar on the right. Bins from left (top) to right (bottom) correspond to 20 logarithmically-spaced bins of  $w_p(r_p)$  from  $r_p=0.3 h^{-1}$  Mpc to  $r_p=30.0 h^{-1}$  Mpc and 20 linearly-spaced bins of  $p(N_8^g)$  from  $N_8^g=0.0$  to  $N_8^g=160.0$ .

We use the jackknife resampling technique to compute covariance matrices for our observables. In our analysis we utilize measurements from the SDSS galaxy sample as well as a mock sample derived from the ELUCID simulation. In either case we compute two jackknife resampled covariance matrices, one for  $w_p$  and  $p(N_8^g)$  and the other for the five  $N_8^g$ -selected correlation functions  $w_p(r_p|\tilde{N}_8^{g,i})|_{i=1-5}$ . Using multiple realizations of our ELUCID mock sample we have computed the contribution to the covariance from using a single random realization of the HOD. We have found that this realization contribution to the error is strongly subdominant at all scales for all of our observables and is therefore ignored.

The covariance matrices computed on different mocks

and the SDSS catalog generally exhibit similar behaviors. However, it should be noted that quantitatively there are important differences. The sample variance for our observables will obviously scale with their signal, but the presence or absence of assembly bias will also have an effect. Two mocks with the same signal but different values of our assembly bias parameters will have different observable covariance matrices. If we consider the example of  $w_p$ , we see that these two mocks will have different covariances because assembly bias is adding to the spatial variation of  $w_p$  due to the large scale density. In the case of the distribution of  $N_8^g$ , the effect is even more direct because any galaxy assembly bias acts to boost the variance of  $N_8^g$ .

The correlation matrices measured in SDSS for  $\{w_p, p(N_8^g)\}$  and  $w_p(r_p|\tilde{N}_8^{g,i})|_{i=1-5}$  are shown in Figure A1 and A2, respectively. Turning towards Figure A1 we see that for  $w_p$  there are significant correlations among bins within the 1-halo regime and bins within the 2-halo regime, but there is little correlation between bins across these two regimes. For  $p(N_8^g)$  we see that the covariance is mostly diagonal with minor correlations between nearby bins. We also see that there are negative correlations between large and small  $N_8^g$  bins. This reflects the explicit integral constraint on the probability distribution function.

Overall, the covariance between the two types of observables is weak but exhibits some structure. There are negative covariances between all bins of  $w_p$  and bins of low  $N_8^g$  and positive covariance between all bins of  $w_p$  and bins of high  $N_8^g$ . This is because galaxies with high values of  $N_8^g$  are in high density regions and therefore have stronger clustering, while those with low values of  $N_8^g$  are in low density regions and have weaker clustering.

Figure A2 shows the correlation matrix of our five  $N_8^g$  selected correlation functions. Going from left to right, the correlation matrix for increasing quintiles of  $N_8^g$  starts with the bottom quintile on the far left and ends with the top quintile on the far right. In all cases we see roughly the same structure we observe for the global  $w_p$ , there are significant correlations between nearby bins but little correlation between large and small scales. Additionally, the low-quintile correlation functions are more diagonally dominated than the high-quintile correlation functions. This is because the shot-noise component, which is diagonal and constant across the five quintiles, becomes more dominant when the sample-variance component, which scales with the signal, is weaker. Using jackknife resampling we have also calculated the covariance between our five  $N_8^g$  selected cross-correlation functions. We have found these errors to be extremely noisy



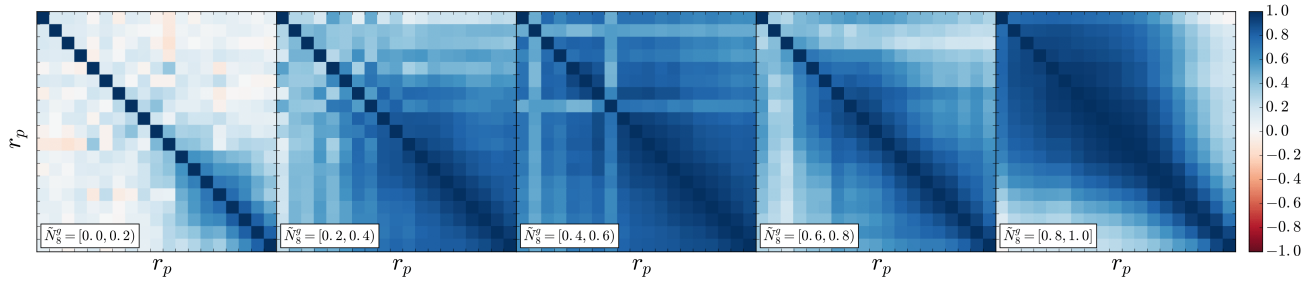


**Figure A2** Correlation matrix of the projected cross-correlation function between galaxy quintiles selected by  $N_8^g$  and the overall galaxy sample,  $w_p(r_p | \tilde{N}_8^{g,i})_{i=1-5}$ , with the correlation coefficients colour-coded by the colour bar on the far right. In each panel bins from left (top) to right (bottom) correspond to 20 logarithmically-spaced bins of  $w_p(r_p | \tilde{N}_8^{g,i})$  from  $r_p=0.3 h^{-1}$  Mpc to  $r_p=30.0 h^{-1}$  Mpc.

**Table B1** Posterior constraints of model parameters from an ELUCID mock catalog with significant levels of galaxy assembly bias used as data. Likelihood's are calculated using ELUCID and Bolshoi haloes with  $Q_{\text{cen}}$  and  $Q_{\text{sat}}$  fixed to zero. Values quoted are posterior modes with 68% confidence intervals. The value of  $\chi^2/\text{d.o.f}$  is calculated from the mean of the posterior samples. Input values are listed in the last row.

| Data vector   | Haloes  | $\sigma_{\log M}$      | $\log M_{\min}$         | $\log M_1$              | $\alpha$               | $Q_{\text{cen}}$ | $Q_{\text{sat}}$ | $\mathcal{A}_{\text{con.}}$ | $\chi^2/\text{d.o.f}$ |
|---|---------|------------------------|-------------------------|-------------------------|------------------------|------------------|------------------|-----------------------------|-----------------------|
| $\{w_p(r_p), n_g\}$                                       | ELUCID  | $0.20^{+0.17}_{-0.13}$ | $12.00^{+0.06}_{-0.05}$ | $13.00^{+0.11}_{-0.12}$ | $0.90^{+0.09}_{-0.08}$ | -                | -                | $0.85^{+0.12}_{-0.12}$      | 13.01/16              |
| $\{w_p(r_p), n_g\}$                                       | Bolshoi | $0.19^{+0.17}_{-0.13}$ | $12.01^{+0.06}_{-0.06}$ | $12.80^{+0.11}_{-0.12}$ | $0.80^{+0.08}_{-0.08}$ | -                | -                | $0.87^{+0.12}_{-0.12}$      | 42.23/16              |
| $\{w_p(r_p), p(N_8^g), n_g\}$                             | ELUCID  | $0.26^{+0.10}_{-0.10}$ | $12.03^{+0.06}_{-0.05}$ | $12.79^{+0.08}_{-0.09}$ | $0.80^{+0.06}_{-0.06}$ | -                | -                | $0.81^{+0.13}_{-0.12}$      | 36.99/36              |
| $\{w_p(r_p), p(N_8^g), n_g\}$                             | Bolshoi | $0.19^{+0.12}_{-0.11}$ | $11.97^{+0.05}_{-0.04}$ | $12.72^{+0.07}_{-0.07}$ | $0.79^{+0.05}_{-0.05}$ | -                | -                | $0.86^{+0.12}_{-0.12}$      | 54.51/36              |
| $\{w_p(r_p   \tilde{N}_8^{g,i})_{i=1-5}, n_g\}$           | ELUCID  | $0.16^{+0.06}_{-0.07}$ | $12.03^{+0.03}_{-0.03}$ | $12.96^{+0.08}_{-0.09}$ | $0.85^{+0.05}_{-0.05}$ | -                | -                | $0.74^{+0.12}_{-0.14}$      | 65.38/96              |
| $\{w_p(r_p   \tilde{N}_8^{g,i})_{i=1-5}, n_g\}$           | Bolshoi | $0.17^{+0.07}_{-0.07}$ | $12.01^{+0.03}_{-0.03}$ | $12.81^{+0.07}_{-0.09}$ | $0.79^{+0.04}_{-0.05}$ | -                | -                | $0.69^{+0.14}_{-0.15}$      | 141.51/96             |
| $\{w_p(r_p   \tilde{N}_8^{g,i})_{i=1-5}, p(N_8^g), n_g\}$ | ELUCID  | $0.20^{+0.07}_{-0.07}$ | $12.00^{+0.03}_{-0.02}$ | $12.84^{+0.05}_{-0.06}$ | $0.83^{+0.04}_{-0.04}$ | -                | -                | $0.71^{+0.14}_{-0.14}$      | 96.57/116             |
| $\{w_p(r_p   \tilde{N}_8^{g,i})_{i=1-5}, p(N_8^g), n_g\}$ | Bolshoi | $0.18^{+0.08}_{-0.08}$ | $11.96^{+0.03}_{-0.02}$ | $12.75^{+0.04}_{-0.05}$ | $0.81^{+0.03}_{-0.04}$ | -                | -                | $0.69^{+0.15}_{-0.16}$      | 175.98/116            |
| Input Value   | -       | 0.20                   | 11.95                   | 13.15                   | 1.0                    | -0.50            | 0.50             | 0.86                        | -                     |

and near zero. Therefore we chose to set them equal to zero in what follows.

## Appendix B Model Tests with Standard Halo Occupation Distribution

In section 6 we performed a variety of mock tests using two ELUCID mocks, one without and the other with strong galaxy assembly bias. During those mock

tests, we allow  $Q_{\text{cen}}$  and  $Q_{\text{sat}}$  to vary freely. For the sake of completeness here we include analogous mock tests by fitting a standard HOD model with fixed values of  $Q_{\text{cen}} = Q_{\text{sat}} = 0$  to the ELUCID mock with strong galaxy assembly bias ( $Q_{\text{cen}} = -0.50$ ,  $Q_{\text{sat}} = 0.50$ ). The results of these mock constraints are listed in Table B1; values quoted correspond to parameter posterior modes and 68% confidence intervals. Input values for the HOD parameters are listed in the final row of the table.